



Czech Technical University in Prague
Faculty of Mechanical Engineering
JOSEF BOŽEK CENTER OF VEHICLES FOR SUSTAINABLE MOBILITY

1-D Model of Radial Centripetal Turbine with Twin Scroll

Author: Prof. Ing. Jan Macek, DrSc.
e-mail: jan.macek@fs.cvut.cz

Address: ČVUT – FS, Ú 12201
Technická 4
CZ-166 07 PRAHA 6

Report U 12201 Z 14 – 02
Prague, February 2014

Contents

| | |
|--|----|
| Contents | 2 |
| Abstrakt | 3 |
| Abstract | 3 |
| Introduction | 4 |
| 1-D Modular Model for a CR Turbine Map Simulation | 5 |
| 1D Model of a Dissipative, Rotating Flow | 5 |
| The Elements of a Model..... | 5 |
| 2-D Axial or Radial Flow with Tangential Velocity Component..... | 6 |
| Model of a CR Turbine..... | 6 |
| Static Pressure Conditions | 7 |
| Pressure and Temperature Linking Conditions | 7 |
| Flow Rate Linking Condition | 7 |
| Features of CR Turbine with Different Sized Exducers | 12 |
| Turbine with a Twin-Entry Inlet Scroll for Pulse Exhaust Systems..... | 17 |
| New Turbine Modular Model with Pre-Defined Mass Flow-Rates | 23 |
| Turbine Map Parameters | 27 |
| Enthalpy Head at a Turbine | 27 |
| Other CRT Performance Parameters | 28 |
| Tuning Parameters | 29 |
| Examples of the First Results | 30 |
| Definitions, Acronyms and Abbreviations..... | 37 |
| SYMBOLS | 37 |
| INDECES | 37 |
| ACRONYMS..... | 38 |
| Appendix 1 | 39 |
| The Flow in Basic Passive Elements and Definition of Tuning Coefficients | 39 |
| 2-D Cases Transformed to 1-D..... | 39 |
| The Accelerated Flow in Nozzles..... | 40 |
| A Vaneless Nozzle for a Radial Turbine | 43 |
| The Flow in a Rotating Channel | 44 |
| Decelerated Flow in Diffusers | 45 |
| AN OUTLEt axial-radial diffuser..... | 46 |
| Flow Junctions | 47 |
| Incidence Loss of a Turbine Impeller | 48 |
| Appendix 2 – Examples of Turbine Models Built by Entities of 1-D Code | 49 |
| References..... | 51 |

Abstrakt

Zpráva popisuje práce vykonané při simulačním rozboru optimalizace radiálních strojů se zřetelem na podmínky práce ve dvoustupňové skupině přeplňovaných spalovacích motorů.

Obsahuje postup předběžné optimalizace dvoustupňové skupiny na základě algebraického modelu, obsahujícího základní regulační prvky turbin i kompresorů (obtoky a pohyblivé lopatkování), EGR a tlakové ztráty mezi stroji. Optimalizace se prozatím provádí pod řízením komerčního optimalizátoru s genetickým algoritmem.

Dále je ve zprávě popsán algebraický model dějů v turbině na střední proudnici, kalibrovatelný podle experimentů a přenositelný do 1-D nestacionárních řešičů (ověřeno na GT Power). Model v současné podobě umožňuje extrapolaci naměřených charakteristik turbin. Z uvedených příkladů simulací vyplynulo, že známé snížení účinnosti regulovatelných turbin je z části způsobeno nesladěním průřezu rozváděcího ústrojí a výstupníku.

Dále se řeší interakce proudů ve dvoustupňovém rozváděcím ústrojí pro pulsační výfukové systémy, která je významná u vysokotlakých turbin s přirozeně zvýšeným vlivem pulsací ve výfuku pro jejich účinnost.

Abstract

The report describes a way to a 1-D central streamline model of a radial turbine flow and energy transformation. The original model finding dependence of flow-rate on pressure ratio was amended by twin-scroll nozzles (both vaneless or with blade cascades) and mixing individual partition flows upstream of additional vaneless nozzle. This model is transferrable to GT Power using GTP modules based 1-D unsteady solvers. Nevertheless, the original central streamline steady flow model has not been sufficiently converging. Therefore, new modular model based on inversed pressure – mass flow-rate approach has been developed. It has suitable features even for more detailed description of turbine flows and energy transformation. The first results of pulse influence on turbine maps delivered expected results consisting in complicated interaction between individual losses.

These features call for appropriate optimization of turbines for high pulsation factor, as it is used for twin-scroll four cylinder engine turbochargers (two cylinders with 360° distance between pulses). The results of turbine matching should be used in turbine design. The force of the model created is especially in this transfer of turbine features found during mapping back to the design stage at a turbocharger manufacturer. The model itself is not fully predictive, using experimentally or in CFD found loss coefficient but it is suitable for extrapolation before detailed CFD simulation or experiments are done.

Introduction

Matching of a turbocharger to an IC engine is still a demanding task, especially if more complicated lay-out of two-stage turbocharging is used. The first part of this report summarizes the current approaches at different levels of complexity.

Centripetal radial turbines (**CRT**) of combined radial-axial flow are commonly used in small and medium turbochargers. Their advantageous features are the comparatively high isentropic efficiency (η_{Ts}) even at small impeller diameters and a compact cheap design including a variable geometry (**VG**) turbine. Nevertheless, they feature some disadvantages as well. Without speaking about design mechanical problems, their aerodynamic design is complicated due to the pure 3-D nature of flow. The thermodynamic optimization of the turbocharger-to-engine tuning differs from the standard axial turbine matching procedure due to the turbine-speed dependence of flow rate.

Current demands call for a more deep approach. The problem of optimization is closely connected to appropriate simulation. The recent design of a VG nozzle brings another degree-of-freedom to turbocharger operation which is welcome. Nevertheless, it does the same for the optimization procedure and its data demands. Measurements of all data needed for the turbine description are often not available in the full range. The complex data set acquisition requires expensive test equipment (high-speed dynamometer or set of nonstandard compressor impellers) and a powerful source of pressurized air. These problems have been known for years – [1].

Moreover, VGT usage causes another important issue – the reduction of efficiency caused not only by nozzle leakage flows but also by off-design operation of impeller, which should be matched to variable position of nozzle blades, as well. The contribution of some degree of impeller flow variability should be modelled before it is designed and tested.

Turbocharger interaction with a reciprocating engine cycle must take into account typical operation regimes including transient operation. Cycle simulation provides efficient help here – [2]. Well-optimized matching of a CR turbocharger to an ICE is rather complicated due to the strong dependency of its discharge coefficient on a blade-speed ratio $x=u/c_s$ (*impeller circumferential velocity / velocity after isentropic expansion of a total enthalpy head*), which is especially important for pulse exhaust manifolds. This feature, uncommon at axial turbines, for which current optimization methods were developed, has to be respected because of its influence on instantaneous turbine power and exhaust manifold pressure history. The realistic prediction of instantaneous isentropic efficiency fulfills the second condition for turbine simulation including the influence of transonic flow effects at very high pressure ratios.

Section-divided pulse exhaust manifolds and longitudinal (circumferential) splitting of a twin-entry turbine scroll and nozzle create other problems due to the partial admission and the mixing of both flows upstream to a turbine impeller. Unlike a standard radial-split axial-turbine nozzle ring a scroll baffle performs as a pulse-converter tongue possibly even causing ejector effects. Off-design incidence angle and off-design turbine reaction are additionally influenced by a variable nozzle vanes position in the case of VG turbines. For these reasons the current report is devoted to solving the outlined problems of thermodynamic simulation based on experimental data currently available in the simple form of algebraic models, suitable for being involved into the whole system of two-stage group.

The aims of this contribution are therefore:

- ☐ to develop a 1-D modular model of a radial centripetal turbine suitable for direct use in 1-D engine simulation codes (e.g., using modules of GT Power);
- ☐ to develop a twin-scroll turbine model respecting the features of pulse operation based on aerodynamics, not just combining look-up table models for interpolation, as it has been done in the current versions of simulation codes;

The implementation of the results into comprehensive engine-simulation systems is possible either using concentrated data in the form of standard universal turbine characteristics or using new specific modules similar to a pipe-connection module.

The latter case seems to be more suitable because of multi-parameter substance of turbine characteristics. It covers complicated flow interactions in divided pulse exhaust manifolds with twin-entry turbine nozzles. Moreover the developed modules make possible a description of a turbine interaction with sophisticated semi-active parts of piping like an outlet axial-radial diffuser.

An original multi-parametric calibration method has been developed to find empirical parameters of the model and it has been tested by experiments. Thus the well-based extrapolation of test data outside the range of experiments is possible using the simulation model. This is necessary especially when simulating unsteady states during the pulse operation of a turbine or an off-design turbine performance during transients of an engine.

1-D Modular Model for a CR Turbine Map Simulation

The model (Fig. 1) consists in a substitution of real 3-D flows in a turbine scroll with initial acceleration ($1'-1S'$, in the case of twin-entries additionally $1''-1S''$), an acceleration in a vaneless or bladed nozzle ring ($1S'-2'$, etc.). After transforming a velocity to a rotating impeller and accounting for an incidence loss ($2N-2I$ -rel2I) the relative expansion under centrifugal force influence is simulated (rel2I-rel3I). An exit loss concerns a transformation to fixed coordinate system (rel3I-3). The turbine is sometimes supplemented by an outlet diffuser (3-4) that decelerates a flow in axial and/or radial direction. In all radial flows tangential (vortex) velocity component may be present. In such a case, angular momentum conservation must be added to the standard gas-dynamics principles.

1D Model of a Dissipative, Rotating Flow

A 1-D method has been developed for compressible dissipative flows through rotating channels and under the influence of tangential flow velocity component. It proved to be suitable for a turbine simulation after tuning coefficients had been used. Therefore, the method has been adapted for a calibration of these tuning parameters, evaluating them from experiment data.

The Elements of a Model

The simulation of main turbine elements concerns both nozzle and diffuser 1-D flows, optionally combined with the influence of a rotation of a channel. The form of the model modules is prepared for iterative procedures needed after they are linked to the complex turbine model that is presented later. The equations of basic modules, 1-D passive elements, are described in Appendix 1.

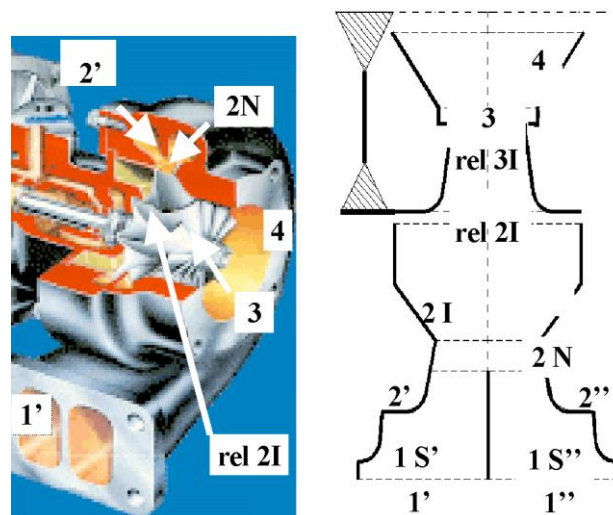


Fig. 1 The simplification of a turbine to a 1-D model (a nozzle exit...2N; an impeller inlet ...2I or rel 2I in a rotating channel; an impeller exit...3 or rel 3I; an outlet diffuser exit 4 – if used). See also Fig. 2.

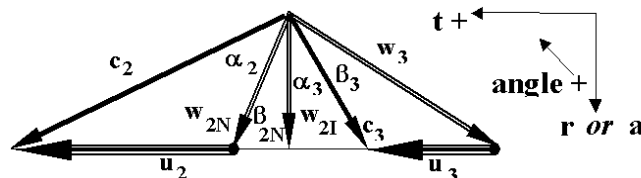


Fig. 2 Turbine velocity triangles at nozzle exit...2, impeller inlet ...2I or impeller exit ...3 for absolute velocities c , relative velocities w and circumferential velocities u

The main idea of their description using mass, energy and angular momentum conservation, consists in incompressible fluid dynamics equations corrected by a iterative coefficient to fluid compressibility. The isentropic efficiency (or loss

coefficient complementing its definition) characterizes a kinetic energy dissipation in blade cascades – see Appendix 1, Fig. 25 and Fig. 26 or Fig. 28 and equations (62) - (64).

2-D Axial or Radial Flow with Tangential Velocity Component

It features some special properties. The conservation of total enthalpy in a relative flow through a rotating channel yields (\mathbf{w} is a velocity relative to the coordinate system, rotating with a circumferential velocity \mathbf{u} ; no work is done in this coordinate system unlike in an absolute one)

$$h + \frac{w^2}{2} - \frac{u^2}{2} = \text{const.} \quad (1)$$

The specific power in an absolute coordinate system, where certain work may be done due to the movement of channel walls, is obviously given by

$$\Delta \left(h + \frac{c^2}{2} \right) = \Delta h_0 = \frac{P_T}{\dot{m}} = u_2 c_{t2} - u_3 c_{t3} \quad (2)$$

The Euler turbine equation was applied at the right-hand side using tangential components of absolute velocities according to velocity triangles in Fig. 2 (see coordinate system axes). In the role of a flow-rate determining coordinate the radial or axial ones are used at an impeller radial inlet or an axial impeller exducer outlet, respectively. The angles are measured from the flow direction, i.e., from radial or axial ones. All directions of flow are quite general, only the inlet angle at impeller blades is 0 deg, i.e., radial vanes are assumed at inlet as it is a standard case.

The specific case of a vaneless nozzle ring, a radial-axial diffuser with rotating flow or those an incidence loss at an impeller inlet are described in details in Appendix 1.

Model of a CR Turbine

After all the elements of a turbine have been developed (see Appendix 1) the construction of a turbine model can start. The kinematic conditions have been presented in FIG. 2. An h - s diagram in FIG. 3 presents the transformation of an energy inside a turbine together with lost enthalpy heads Δh_N , Δh_I (the loss coefficients of a nozzle ring and impeller are ζ_N or ζ_I and efficiencies η_N , η_I respectively, see Appendix 1. An additional loss is caused by an off-design angle of attack at an impeller inlet $\Delta h_{I \text{ loss}}$.

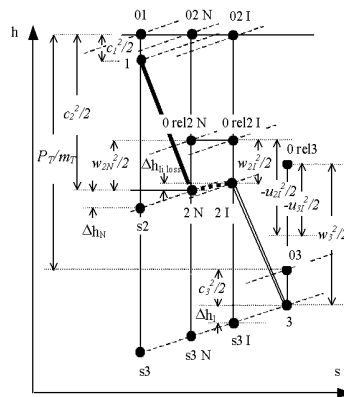


Fig. 3 Enthalpy-entropy diagram of centripetal radial turbine process

Conditions of element linking at their boundaries are given by equivalence of shared

- ☐ flow rates (mass conservation) – leakages at impeller and partial flow via exducer by-pass;
- ☐ static enthalpies (energy conservation);
- ☐ absolute velocities (momentum conservation) and kinetic energies belonging to them (energy conservation);
- ☐ static pressures (momentum or angular momentum conservation).

Enthalpies and velocities transformed according to vector sums in Fig. 2 cause no problems in linking, other issues will be commented.

Static Pressure Conditions

Static pressures are the same at boundaries of elements. An empirical equation for a pressure loss due to the off-design incidence angle at impeller (radial) blades was added - see Fig. 2 and Fig. 3. The simplest approach for radial blades concerns dissipation of all kinetic energy associated with tangential relative velocity component (Benson, $\zeta_{II} = \tan \beta_{2I}$, see e.g. [1]). Usually, $\beta_{2I} = \beta_2$ was used. The experimental results call for correction of this simple approach, as stated already in [3], because negative angles of attack feature lower losses. Using the idea of a relative impeller vortex, the flow should be declined opposite to the sense of rotation. It qualitatively agrees with the experience of slight negative incidence angle, as stated above - see p. 48. In this specific case, neither static pressures nor stagnation pressures are the same if passing the interface **2** between nozzle exit and impeller inlet.

Pressure and Temperature Linking Conditions

In general, static parameters are the same at any interface between modules of the model with the above mentioned exception of static pressure and temperature influenced by incidence angle. Otherwise, due to the necessity to describe the flow in relative and absolute coordinates, the total and stagnation states have to be transformed. The subscript **0** means stagnation state in absolute coordinates, which is equal to stagnation state. Stagnation temperature (in fact, stagnation enthalpy) is conserved for any stator part of blades. Stagnation pressure is stepwise reduced due to pressure losses (entropy increase). In the case of twin-scroll, superscripts **I** or **II** are used for the partitions of scroll.

In an impeller, **rel 0** subscript means stagnation state in relative coordinate system. Stagnation temperature (enthalpy) is not conserved if potential energy in the field of centrifugal forces is changed (i.e., in the case of radius change).

The subscript **2N** is used to stress the position just close to nozzle exit and it may be coupled with absolute **or** relative state transformed to impeller coordinates. relative nozzle exit state is important to find relative state upstream of incidence loss. **2I** means impeller inlet, always in relative coordinates after incidence loss of impeller blades took place.

Flow Rate Linking Condition

Quick convergent iterative procedure can be applied for subsonic flow – non-compressible flow approximation is calculated directly fulfilling the continuity equation for both turbine nozzles in a series, i.e., for both nozzle ring (or a vaneless nozzle, if used) and an impeller with correcting terms **C**. The by-passed exducer flow is assumed to be known in advance (and controlled by throttling at outlet in practice). Small leakages – both influenced by centrifugal force field close to blades or independent on it (just throttling through a clearance) are iterated during calculation.

$$A_{rN2} \cos \alpha_2 C_N \frac{p_{01}}{\sqrt{rT_{01}}} \sqrt{2\eta_N \left(1 - \frac{p_{2N}}{p_{01}}\right)} = A_{aI3} (1 - K_{Isep}) \cos \beta_3 C_I \sqrt{2\eta_I \frac{p_{2N}}{rT_{2N}} \left[\left(p_{2N} + \frac{p_{2N}}{2rT_{2N}} w_{2I}^2 - p_3 \right) - \frac{p_{2N}}{2rT_{2N}} (u_2^2 - u_3^2) \right]} \quad (3)$$

This simplified continuity equation yields (the left term – incompressible nozzle flow with **C_N** correction to compressibility, the right-side term – that of impeller flow with **C_I** correction to compressibility and to leakage and by-pass flows)

$$A_{rN2} \cos \alpha_2 C_N \frac{p_{01}}{\sqrt{rT_{01}}} \sqrt{2\eta_N \left(1 - \frac{p_{2N}}{p_{01}}\right)} = A_{aI3} (1 - K_{Isep}) \cos \beta_3 C_I \sqrt{2\eta_I \frac{p_{2N}}{rT_{2N}} \left[\left(p_{2N} + \frac{p_{2N}}{2rT_{2N}} w_{2I}^2 - p_3 \right) - \frac{p_{2N}}{2rT_{2N}} (u_2^2 - u_3^2) \right]} \quad (4)$$

(4) yields a quadratic equation for **p_{2N}**

$$0 = \frac{2\eta_I (A_{aI3} (1 - K_{Isep}) \cos \beta_3 C_I)^2}{rT_{2N}} \left[\left(1 + \frac{w_{2I}^2}{2rT_{2N}} \right) - \frac{u_2^2 - u_3^2}{2rT_{2N}} \right] p_{2N}^2 + \left[\frac{2\eta_I (A_{rN2} \cos \alpha_2 C_N)^2}{rT_{01}} p_{01} - \frac{2\eta_I (A_{aI3} (1 - K_{Isep}) \cos \beta_3 C_I)^2}{rT_{2N}} p_3 \right] p_{2N} - \frac{2\eta_I (A_{rN2} \cos \alpha_2 C_N)^2}{rT_{01}} p_{01}^2 \quad (5)$$

The quadratic equation (5) can be solved only if $D \geq 0$. Moreover, $p_{2N} > p_3$ for the validity of (4). The case of backward flow through a turbine (possible at high speed and low pressure in front of nozzle) is not very frequent. It is treated in the current code by assumption of zero flow rate if (5) cannot be solved with results physical valid for the standard flow direction:

$$\begin{aligned}
 A &= \frac{2\eta_I (A_{I3} (1 - K_{Isep}) \cos \beta_3 C_I)^2}{rT_{2N}} \\
 B &= \frac{2\eta_{N1} (A_{rN2} \cos \alpha_2 C_N)^2}{rT_{01}} \\
 D &= [Bp_{01} - Ap_3]^2 + 4AB \left[1 + \frac{w_{2I}^2}{2rT_{2N}} - \frac{u_2^2 - u_3^2}{2rT_{2N}} \right] p_{01}^2 = B^2 p_{01}^2 + A^2 p_3^2 - 2ABp_{01} p_3 + 4ABp_{01}^2 \left[1 + \frac{w_{2I}^2}{2rT_{2N}} - \frac{u_2^2 - u_3^2}{2rT_{2N}} \right] = \\
 &= B^2 p_{01}^2 + A^2 p_3^2 + 2ABp_{01} \left\{ p_{01} \left[2 + \frac{w_{2I}^2}{rT_{2N}} - \frac{u_2^2 - u_3^2}{rT_{2N}} \right] - p_3 \right\} \\
 p_{2N} &= \frac{-[Bp_{01} - Ap_3] \pm \sqrt{D}}{2A \left[\left(1 + \frac{w_{2I}^2}{2rT_{2N}} \right) - \frac{u_2^2 - u_3^2}{2rT_{2N}} \right]} \quad (6) \\
 \text{if } D < 0 \text{ or } \frac{p_{2N}}{p_{01}} > 1 \text{ or } \left(p_{2N} + \frac{p_{2N}}{2rT_{2N}} w_{2I}^2 - p_3 \right) - \frac{p_{2N}}{2rT_{2N}} (u_2^2 - u_3^2) < 0 \text{ or} \\
 \text{or } 2c_{p0rel2} \eta_I \left[1 - \left(\frac{p_3}{p_{0rel2I}} \right)^{\frac{\kappa-1}{\kappa}} \right] + u_3^2 - u_2^2 < 0 \text{ then } \dot{m}_N = \dot{m}_m = 0
 \end{aligned}$$

The last condition is based on the accurate flow-rate through impeller, (17). The leakage flow is neglected in this case. Unknown static temperature T_{2N} and relative radial impeller inlet velocity w_{2I} are iterated together with compressibility&loss correction coefficients C_N and C_I .

Correction coefficients are calculated after one iteration loop is finished. The procedure is simple for nozzle ring assuming no flow separation from blades. The limit for transonic case is calculated with losses (Saint-Venant and Fanno processes)

$$\dot{m}_N = \begin{cases} A_{rN2} \cos \alpha_2 \frac{p_{01} \frac{p_{2N}}{p_{01}}}{rT_{01} \left[1 - \eta_N \left[1 - \left(\frac{p_{2N}}{p_{01}} \right)^{\frac{\kappa-1}{\kappa}} \right] \right]} \sqrt{2r \frac{\kappa}{\kappa-1} T_{01} \eta_N \left[1 - \left(\frac{p_{2N}}{p_{01}} \right)^{\frac{\kappa-1}{\kappa}} \right]} & \text{if } \varepsilon^* = \left[1 - \frac{\kappa-1}{\eta_N(\kappa+1)} \right]^{\frac{\kappa}{\kappa-1}} < \frac{p_{2N}}{p_{01}} \\
 A_{rN2} \cos \alpha_2 \frac{p_{01}}{rT_{01}} \frac{\varepsilon^*}{1 - \eta \left[1 - \varepsilon^{*\frac{\kappa-1}{\kappa}} \right]} \sqrt{2r \frac{\kappa}{\kappa-1} T_{01} \eta_N \left[1 - \varepsilon^{*\frac{\kappa-1}{\kappa}} \right]} & \text{otherwise} \end{cases} \quad (7)$$

$$C_N = \frac{\dot{m}_N}{A_{rN2} \cos \alpha_2 \frac{p_{01}}{\sqrt{rT_{01}}} \sqrt{2\eta_N \left(1 - \frac{p_{2N}}{p_{01}} \right)}} \quad (8)$$

A more complicated procedure has to be applied for correction of mass-flow rate in the impeller:

1. Transformation of total states from fixed (absolute) coordinate system to rotating (relative) system of impeller: Velocities are calculated at known static pressure and total (stagnation) temperature. Energy conservation and continuity equations yield quadratic equation for static temperature.

$$\begin{aligned}
T_{01} &= T_{02} \\
c_2^2 &= \left(\frac{\dot{m}_N}{A_{rN2} \frac{p_{2N}}{rT_{2N}} \cos \alpha_2} \right)^2 = 2c_p(T_{01} - T_{2N}) \\
\left(\frac{r \dot{m}_N}{A_{rN2} \cos \alpha_2 p_{2N}} \right)^2 T_{2N}^2 + 2c_p T_{2N} - 2c_p T_{01} &= 0 ; \quad T_{2N} = \frac{-c_p + \sqrt{c_p^2 + 2c_p T_{01} \left(\frac{r \dot{m}_N}{A_{rN2} \cos \alpha_2 p_{2N}} \right)^2}}{\left(\frac{r \dot{m}_N}{A_{rN2} \cos \alpha_2 p_{2N}} \right)^2} \\
p_{02N} &= p_{2N} \left(\frac{T_{01}}{T_{01} - \frac{c_2^2}{2c_p}} \right)^{\frac{\kappa}{\kappa-1}}
\end{aligned} \tag{9}$$

2. Relative stagnation parameters before the flow enters interblade channel of an impeller are calculated from energy conservation

$$\begin{aligned}
T_{rel02N} = T_{rel02I} = T_{rel02} &= T_{2N} + \frac{w_{2N}^2}{2c_p} = T_{01} + \frac{w_{2N}^2 - c_2^2}{2c_p} = T_{01} + \frac{(c_2 \sin \alpha_2 - u_2)^2 - c_2^2 \sin^2 \alpha_2}{2c_p} \\
p_{rel02N} = p_{02N} \left(\frac{T_{rel02N}}{T_{01}} \right)^{\frac{\kappa}{\kappa-1}} &= p_{02N} \left(1 + \frac{(c_2 \sin \alpha_2 - u_2)^2 - c_2^2 \sin^2 \alpha_2}{2c_p T_{01}} \right)^{\frac{\kappa}{\kappa-1}}
\end{aligned} \tag{10}$$

3. Correction of impeller inlet relative total pressure influenced by losses due to incorrect incidence angle is done using fixed stagnation temperature (energy conservation) and assumption of fixed static pressure during impeller-flow interaction. Approximation of static temperature at impeller inlet is calculated again from quadratic equation of mass&energy conservation. The accurate value of static temperature, pressure and velocity may be iterated from relations (11) - (13) but due to necessary calibration of incidence loss this procedure is not very useful

$$\begin{aligned}
w_{2I}^2 &= \left(\frac{\dot{m}_I}{A_{rI2} \rho'_{2I}} \right)^2 = \left(\frac{\dot{m}_N - \Delta \dot{m}}{A_{rI2} \frac{p_{2N}}{rT'_{2I}}} \right)^2 = 2c_p(T_{rel02} - T'_{2I}) = 2c_p T_{01} + (c_2 \sin \alpha_2 - u_2)^2 - c_2^2 \sin^2 \alpha_2 - 2c_p T'_{2I} \\
\left(\frac{r(\dot{m}_N - \Delta \dot{m})}{A_{rI2} p_{2N}} \right)^2 T_{2I}'^2 + 2c_p T_{2I}' - 2c_p T_{01} - (c_2 \sin \alpha_2 - u_2)^2 + c_2^2 \sin^2 \alpha_2 &= 0 \Rightarrow T_{2I}'
\end{aligned} \tag{11}$$

If the real density in interblade channel is replaced by density before the incidence loss takes place, the relative incidence angle can be found $\tan \beta_2 = \tan \alpha_2 - \frac{u_2}{w_{2I}'^2}$ and

$$\zeta_{I,inc} = 2 \frac{p_{rel02N} - p_{rel02I}}{p_{2N} w_{2I}'^2} = (\tan \beta_2 + K_{imp})^2 = \left(\tan \alpha_2 - \frac{u_2}{w_{2I}'^2} + K_{imp} \right)^2 \tag{12}$$

$$p_{re/02I} = p_{re/02N} - \frac{\zeta_{I,inc} w_{2I}^2 \rho_{2N}}{2}$$

$$p_{2I} = p_{re/02I} \left(\frac{2c_p T_{2N} + w_{2N}^2 - w_{2I}^2}{2c_p T_{2N} + w_{2N}^2} \right)^{\frac{\kappa}{\kappa-1}} ; \quad T_{2I} = T_{re/02} \left(\frac{p_{2I}}{p_{re/02I}} \right)^{\frac{\kappa-1}{\kappa}} ; \quad \rho_{2I} = \frac{p_{2I}}{rT_{2I}} \quad (13)$$

4. Total parameters relative to impeller are calculated from relative motion of a flow in a rotating channel (with potential energy in centrifugal force field). Relative stagnation state is not constant more due to the change of potential energy:

$$c_p T_3 + \frac{w_3^2}{2} - \frac{u_3^2}{2} = c_p T_{re/02} - \frac{u_2^2}{2}$$

$$w_3 = \sqrt{2c_p T_{re/02} \eta_I \left[1 - \left(\frac{p_3}{p_{re/02I}} \right)^{\frac{\kappa-1}{\kappa}} \right] + u_3^2 - u_2^2}$$

$$\rho_3 = \frac{p_3}{rT_{re/02I} \frac{p_{re/02I}}{1 - \eta_I \left[1 - \left(\frac{p_3}{p_{re/02I}} \right)^{\frac{\kappa-1}{\kappa}} \right]}} \quad (14)$$

Transonic limit in a rotating channel is deduced taking into account the influence of centrifugal force:

$$\left(\frac{a^*}{a_{0rel2}} \right)^2 = \frac{2}{\kappa+1} \left(1 - \frac{\kappa-1}{2a_{0rel2}^2} (u_2^2 - u_3^2) \right)$$

$$\varepsilon_I^* = \frac{p_3^*}{p_{0rel2I}} = \left[1 - \frac{1 - \frac{2}{\kappa+1} \left(1 - \frac{\kappa-1}{2a_{0rel2}^2} (u_2^2 - u_3^2) \right)}{\eta_I} \right]^{\frac{\kappa}{\kappa-1}} \quad (15)$$

Then, the main flow component through an impeller is

$$\dot{m}_m = (1 - K_{Isep}) A_{a3I} \cos \beta_3 \rho_3 w_3 \quad (16)$$

and using (14)

$$\dot{m}_m = \begin{cases} (1 - K_{Isep}) A_{a3I} \cos \beta_3 \frac{p_{0rel2I}}{rT_{0rel2}} \frac{p_3}{1 - \eta_I \left[1 - \left(\frac{p_3}{p_{0rel2I}} \right)^{\frac{\kappa-1}{\kappa}} \right]} \sqrt{2c_p T_{0rel2} \eta_I \left[1 - \left(\frac{p_3}{p_{0rel2I}} \right)^{\frac{\kappa-1}{\kappa}} \right] + u_3^2 - u_2^2} & \text{if } \frac{p_3}{p_{0rel2I}} \geq \varepsilon_I^* \\ (1 - K_{Isep}) A_{a3I} \cos \beta_3 \frac{p_{0rel2I}}{rT_{0rel2}} \frac{\varepsilon_I^*}{1 - \eta_I \left[1 - \varepsilon_I^{*\frac{\kappa-1}{\kappa}} \right]} \sqrt{2c_p T_{0rel2} \eta_I \left[1 - \varepsilon_I^{*\frac{\kappa-1}{\kappa}} \right] + u_3^2 - u_2^2} & \text{if } \frac{p_3}{p_{0rel2I}} < \varepsilon_I^* \end{cases} \quad (17)$$

Leakage flow and by-pass flow has to be added separately and included into the main flow correction coefficient. This approach works the better the smaller differences in enthalpy head according to the relation above are present, comparing them to the main flow pressure difference.

$$\dot{m}_I = \dot{m}_m + \Delta \dot{m} \quad (18)$$

$$C_I = \frac{\dot{m}_I}{A_{a/3}(1 - K_{Isep})\cos\beta_3 C_I \sqrt{2\eta_I \frac{p_{2N}}{rT_{2N}} \left[\left(p_{2N} + \frac{p_{2N}}{2rT_{2N}} w_{2I}^2 - p_3 \right) - \frac{p_{2N}}{2rT_{2N}} (u_2^2 - u_3^2) \right]}} \quad (19)$$

The mass conservation yields in more details

$$\begin{aligned} \dot{m}_N &= \dot{m}_I + \Delta \dot{m} \\ \Delta \dot{m} &= \Delta \dot{m}_{I\text{ seals}} + \Delta \dot{m}_{I\text{ shroud}} + \Delta \dot{m}_{by} \end{aligned} \quad (20)$$

The leakage is divided into two types - a piston-ring or labyrinth seal one at the shaft side of a turbine and an open-impeller shroud-side leakage. The former is governed roughly by a static pressure ratio applied to (7) with a throat area calculated from a reference gap width and a discharge coefficient $K_{leak\text{ seal}}$. The latter is calculated with centrifugal force impact, i.e., using a formula similar to (17) with the reference gap area and a discharge coefficient $K_{leak\text{ shroud}}$. These both discharge coefficients become additional tuning parameters.

Features of CR Turbine with Different Sized Exducers

The exducer dimensions cannot be matched in optimum way to different flow-rates and different exhaust gas densities (i.e., for different engine speeds and loads or different rack position of a VGT). The measurements at small VG turbine (C12 CZ a.s.) for two rack positions demonstrate the qualitative change of rated efficiency with opened and closed nozzle blades - Fig. 4.

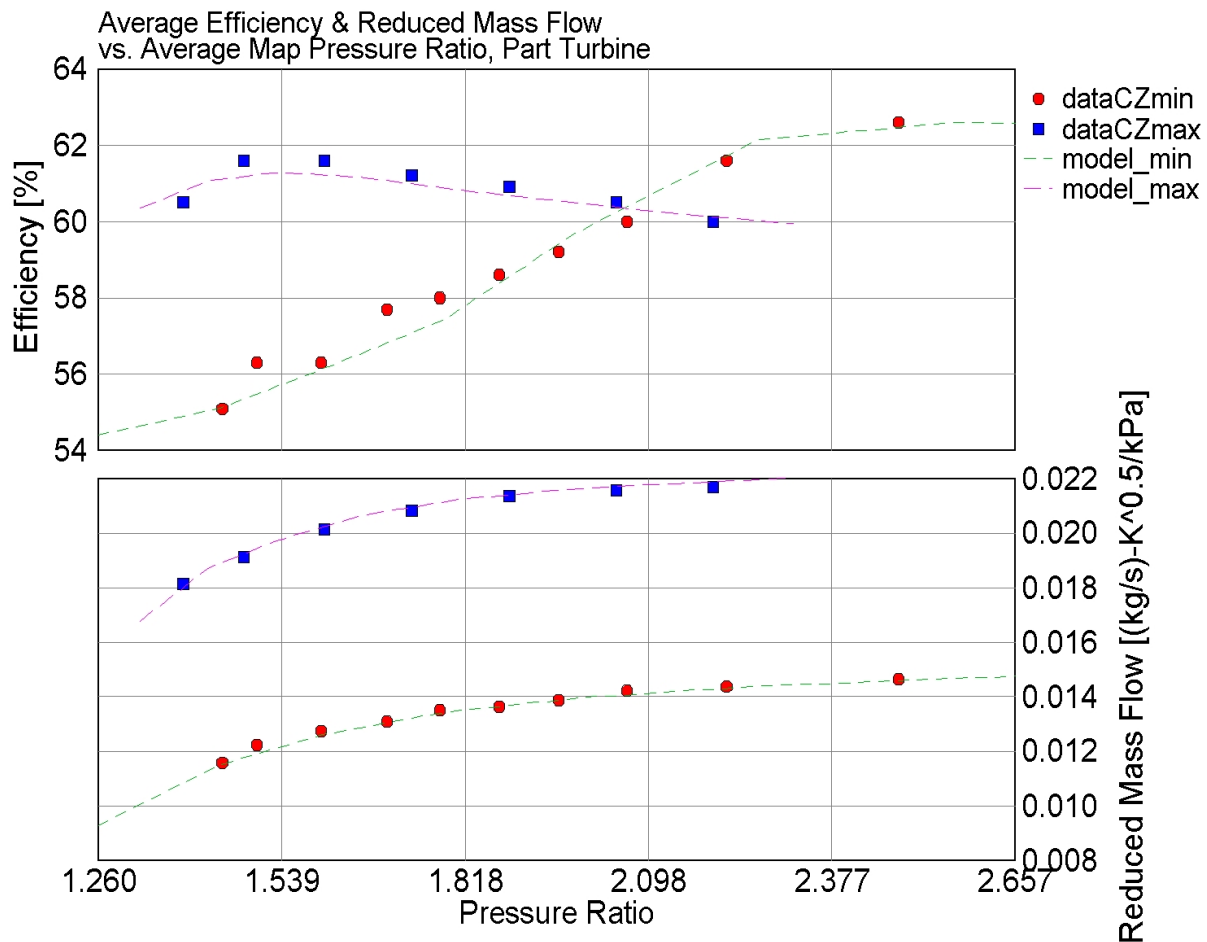


Fig. 4 Rated operational points map of a small VGT for minimum and maximum rack position

The qualitative change of efficiency curve, which increases with pressure ratio, if the nozzle is closed and vice-versa, is clear from it. To understand those dependences better and to check the predictive capability of the current model, these effects were simulated for different nozzle exit angles (rack positions) and exit diameters in the following figures. The calibration coefficients were available for larger K36 size with different trims, therefore this model was used for this introductory validation.

Fig. 5 - Fig. 11 demonstrate the influence of selected parameters, namely the exit angles and exducer exit shroud (outer) diameter. The other calibration parameters except for expansion efficiencies of a nozzle and impeller were kept unchanged. They consider leakage flows (and leakage flow area), correction of incidence angle loss, separation of the flow at exducer outer meridian and impeller windage loss. Moreover, specific speed of a turbine (the qualitative hint for selecting the best shape of impeller form) and turbine reference flow area are presented in the figure descriptions.

The curves at optimum BSR for discharge coefficient μT of a turbine represented by a single nozzle (related to reference flow area), turbine optimum isentropic efficiency and the product of it and turbocharger mechanical efficiency, optimum BSR (u/c_s) itself and Mach numbers at exits from both blade cascades are presented in all figures as a dependence on turbine pressure ratio. Because of iteration controlled manually, not all values have converged fully and some unsmooth curve verteces (especially for Mach numbers) may have occurred.

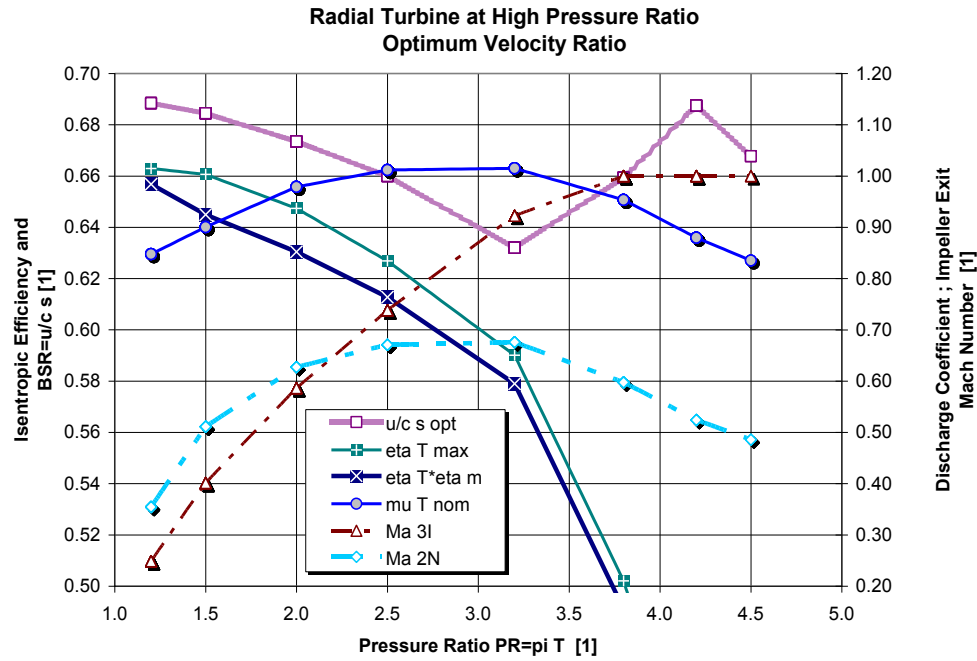


Fig. 5 Rated operational points map of a small radial turbine K36 (impeller inlet diameter 96.5 mm) with the following parameters: nozzle exit angle α_2 63°, impeller exit effective angle β_3 42°, outer exducer diameter D_3 86.6 mm. Other parameters: $n_{q\text{ spec}}$ at PR 3.2 53 min⁻¹, A_{ref} 17.17 cm² (kept at measured value), expansion efficiencies η_N 0.92 and η_I 0.86, K_{inc} 0.8, K_{sep} 22%, K_{wind} 0.09, K_{leak} 0.1+0.1, $A_{\text{leak ref}}$ 1.1 cm²

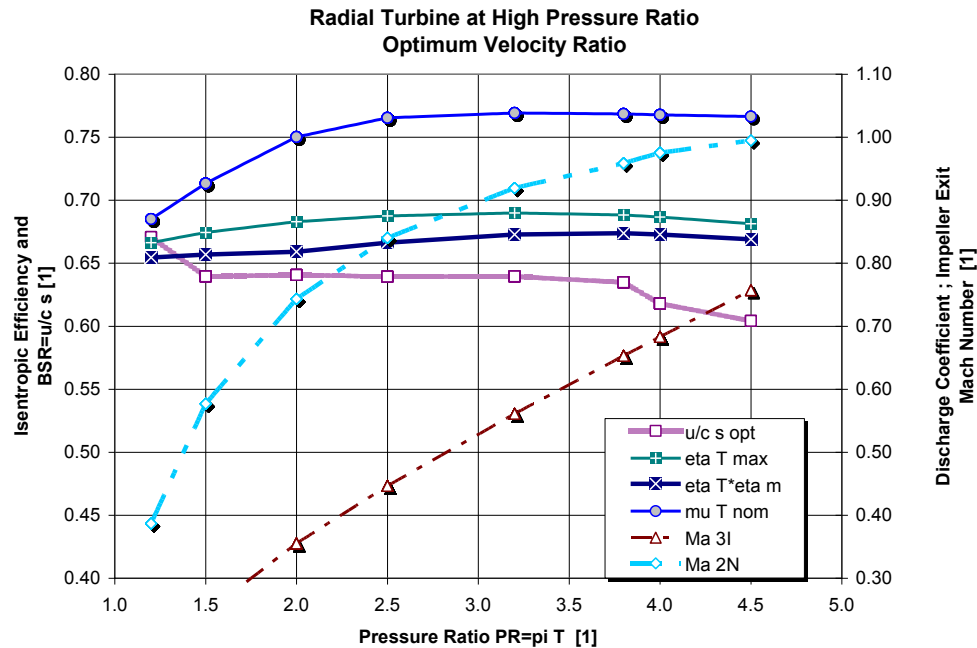


Fig. 6 Rated operational points map of a small radial turbine K36 (impeller inlet diameter 96.5 mm) emulating VGT with partially closed nozzle of following parameters: *partially reduced nozzle exit angle* α_2 75°, β_3 42°, D_3 86.6 mm; $n_{q\text{ spec}}$ at PR 3.2 41.9 min⁻¹, A_{ref} 10.2 cm², *partially reduced expansion efficiency* η_N 0.90, η_I 0.85. Others as in Fig. 5

Fig. 5 - Fig. 7 present the influence of closing nozzle blades from maximum to minimum rack position. The optimum points of the highest isentropic efficiency at fixed turbine inlet temperature 873 K were found during simulations. They approximate the standard closed-loop test results if the conditions for flow in both compressor and turbine are similar, i.e., without turbine choking.

Despite the reduction of expansion efficiency if the nozzle is closed, the turbine efficiency goes up, especially at sufficiently high pressure ratio. While discharge coefficient was kept at the value of 1 for pressure ratio (PR) of 2 approximately, the

reference turbine area A_{ref} reflects the rack position (area of nozzle), which has been presented by reduced mass flow-rate in Fig. 4. At least qualitative accordance with this picture can be found in Fig. 5 - Fig. 7. The Fig. 6 represents the optimum point for the current design of impeller, whereas both extreme cases feature worse efficiency. The effect of choking ($Ma_{3I}=1$) at the impeller with opened nozzle and that at nozzle ($Ma_{2N}=1$) for minimum rack position can be found easily with impact on discharge coefficient, optimum BSR and efficiency. This effect will change closed-loop test results significantly, since a compressor cannot keep a turbine close to optimum BSR if a turbine is choked.

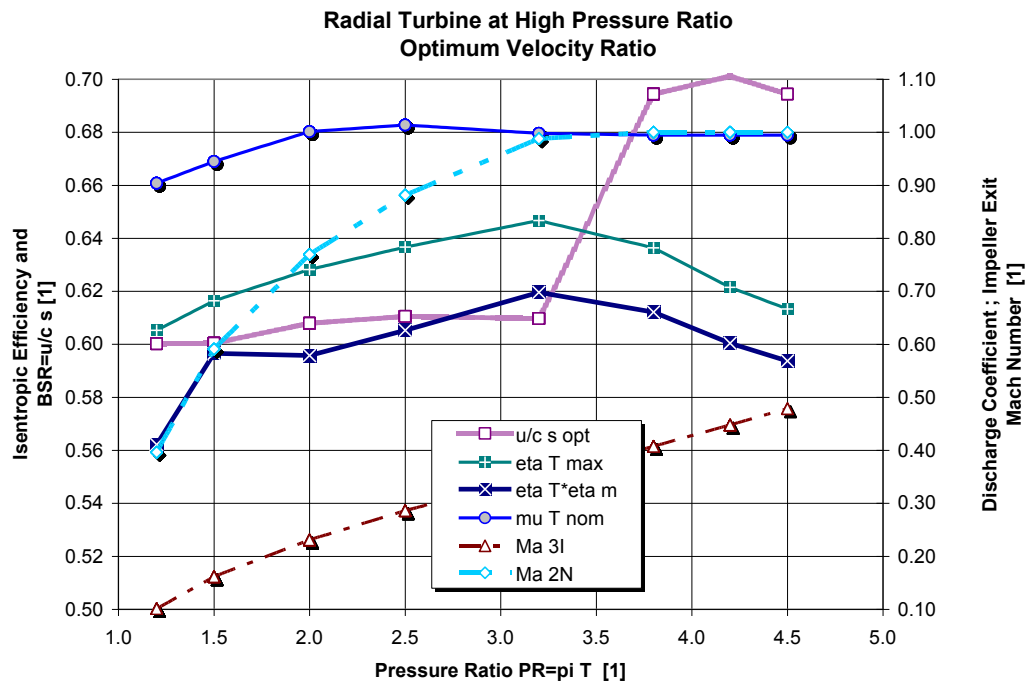


Fig. 7 Rated operational points map of a small radial turbine K36 (impeller inlet diameter 96.5 mm) emulating VGT with closed nozzle of following parameters: fully reduced nozzle exit angle α_2 80°, β_3 42°, D_3 86.6 mm; $n_{q\ spec}$ at PR 3.2 32 min⁻¹, A_{ref} 6.67 cm², reduced expansion efficiency η_N 0.83, η_I 0.85. Others as in Fig. 5

The possibility to change turbine geometry for the minimum rack position are demonstrated in Fig. 9 - Fig. 11. While in Fig. 9 - Fig. 10 the influence of exducer exit angle is studied (following the initial case already shown in Fig. 7), the reduction of exducer shroud diameter is shown in Fig. 11. Again, the results are not ultimately optimized, they demonstrate trends only. The effect of exit area reduction is obvious in both cases, although the change of exit angle is better because of flow direction change accompanying the flow velocity magnitude (changed in the case of diameter variation).

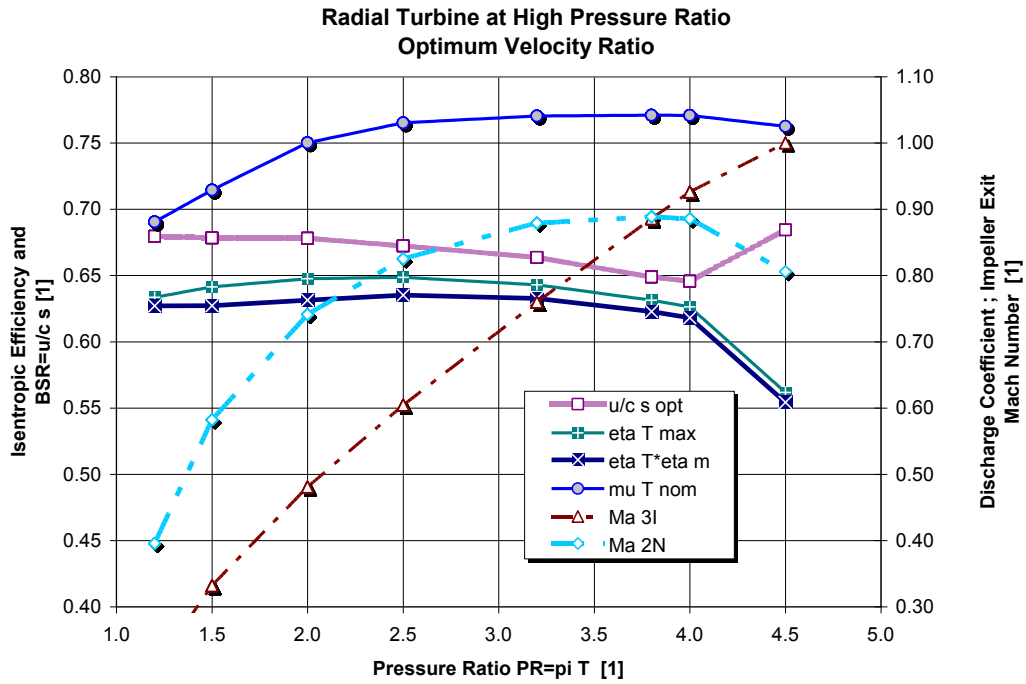


Fig. 8 Rated operational points map of a small radial turbine with fully open nozzle and increased exducer diameter with the following parameters: nozzle exit angle α_2 63° , exducer exit angle β_3 42° , *changed exducer exit diameter* D_3 98 mm, $n_{q\text{ spec}}$ at PR 3.2 57.8 min^{-1} , A_{ref} 18.08 cm^2 , others as in Fig. 5.

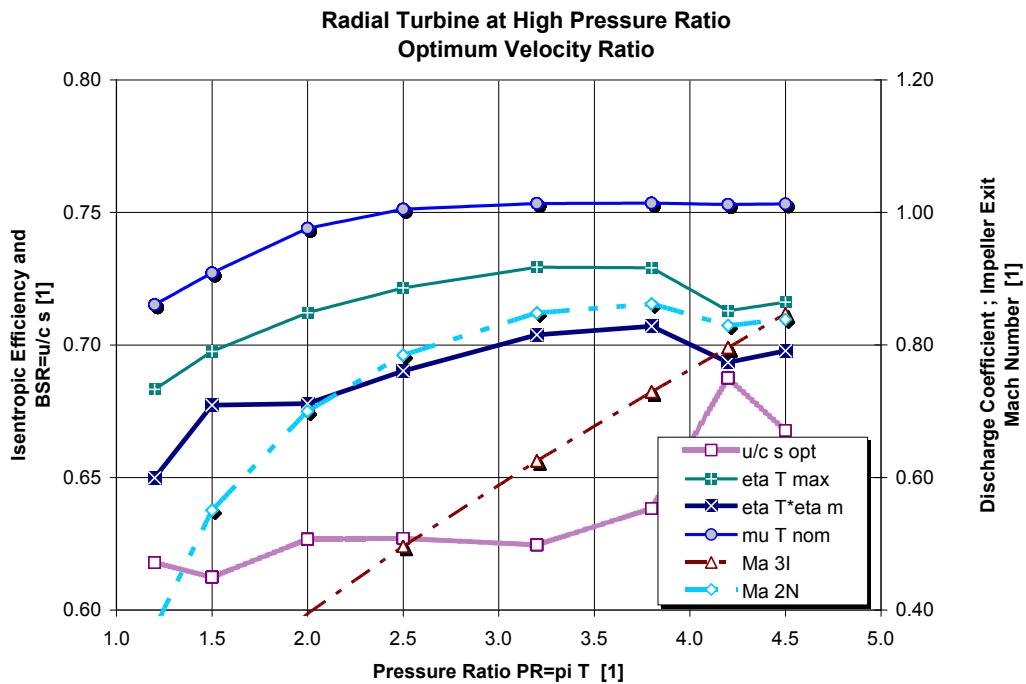


Fig. 9 Rated operational points map of a small radial turbine with reduced nozzle, compare to Fig. 7: reduced nozzle exit angle α_2 80° , reduced impeller exit angle β_3 65° , D_3 86.6 mm, $n_{q\text{ spec}}$ at PR 3.2 32.8 min^{-1} , A_{ref} 6.67 cm^2 , reduced η_N 0.83, η_I 0.85, others as in Fig. 5.

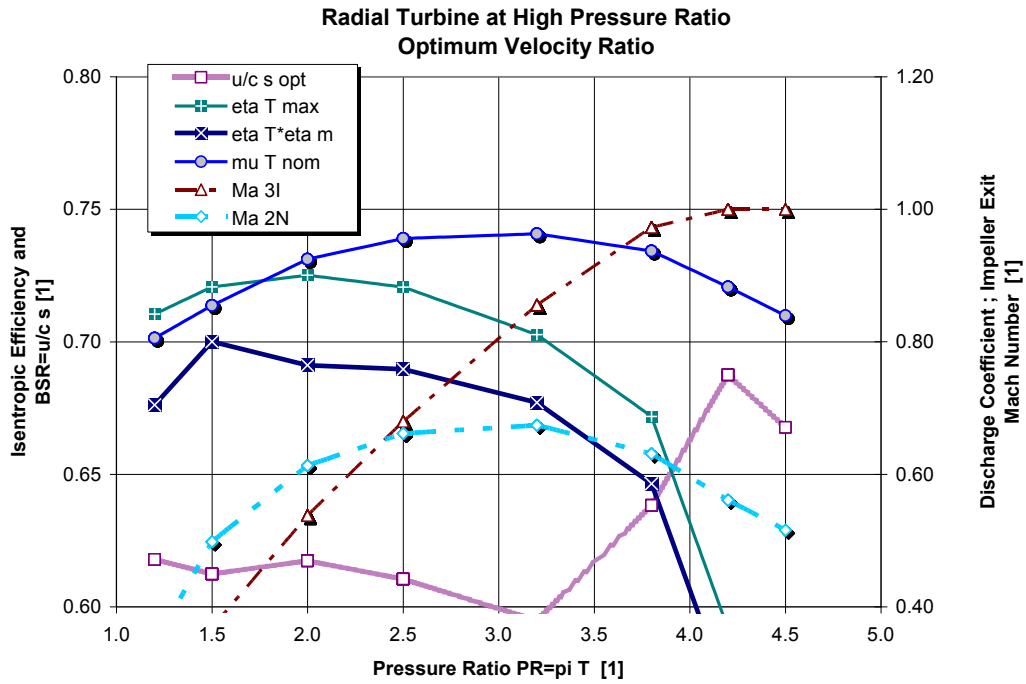


Fig. 10 Rated operational points map of a small radial turbine with the following parameters: *reduced nozzle exit angle α_2 80°, further reduced impeller exit angle β_3 73°, D_3 86.6 mm, $n_{q\text{ spec}}$ at PR 3.2 30.3 min⁻¹, A_{ref} 6.67 cm², reduced η_N 0.83 and η_I 0.85, others as in Fig. 5*

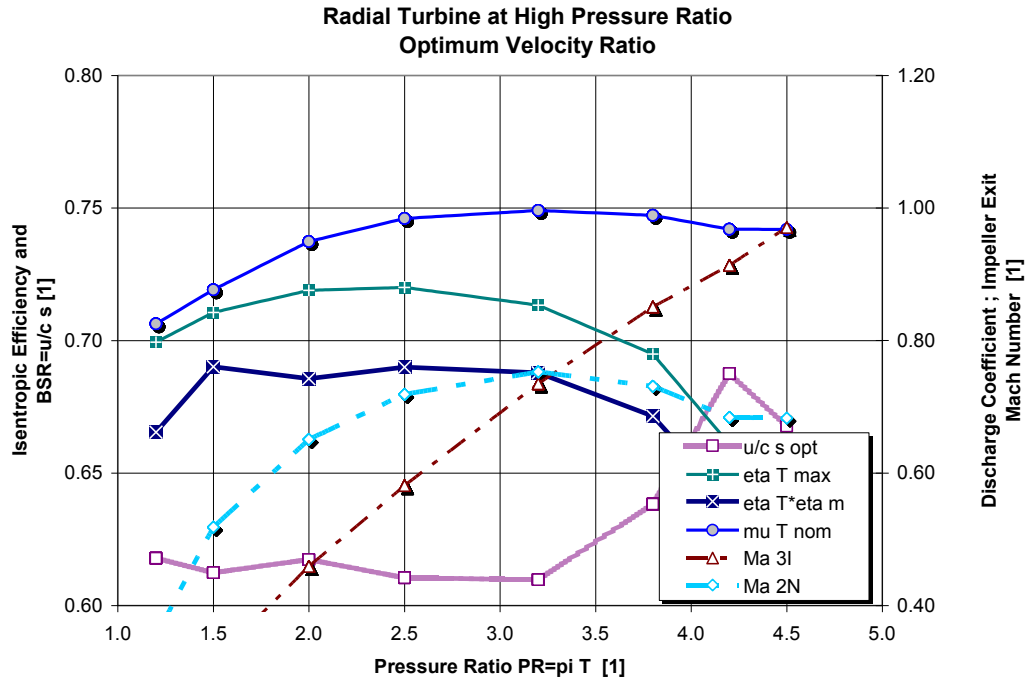


Fig. 11 Rated operational points map of a small radial turbine with the following parameters: *reduced nozzle exit angle α_2 80° and β_3 65°, reduced D_3 80 mm; $n_{q\text{ spec}}$ at PR 3.2 31.5 min⁻¹, A_{ref} 6.67 cm², η_N 0.83 and η_I 0.85, others as in Fig. 5.*

Turbine with a Twin-Entry Inlet Scroll for Pulse Exhaust Systems

Using both vaneless or bladed nozzle rings with pulse exhaust systems, the inlet part of a turbine is divided into sections by a circumferential wall (unlike a twin-entry axial turbine). Most of these turbines are used with three-pulse exhaust systems at 3, 6 or 12 cylinder engines.

A simple model of an axial turbine consists in a calculation of parameters of two fully isolated “turbines” and in their combination weighted by instantaneous flow rates. It is not fully relevant to a radial turbine. Even if no full partial admission occurs, mixing the flows of unequal velocities causes some kinetic energy dissipation. Therefore, a general model of this lay-out, acting as an integrated pulse-converter, has been developed.

The nozzle flow is calculated separately for both parts I_{12} , II_{12} with an outlet pressure $p'_{12} = p''_{12} = p_{12}$. The mixing of two streams downstream a divided turbine nozzle ring or a scroll considers obvious continuity equation and the changes of radial momentum. Angular momentum conservation is incorporated, as well. The former equation yields the static pressure difference between common pressure at scroll outlets and inlet to an impeller, the latter one gives resulting tangential velocity before incidence of uniform flow to an impeller occurs. The different angle of both flows measured in axial plane (and caused by small axial component of inlet velocity) has been neglected in the current model. The presented model assumes known angles of both flows at inlet from separated nozzles α'_{12} and α''_{12} , which is simply possible in the case of blades. In the case of vaneless nozzles, angles can be found by more detailed vaneless scroll described above or just taken into account as calibration parameters.

The numerical solution must be carefully treated because of the presence of some unusual phenomena like reversed flow in a section with pressure lower than that upstream of an impeller, which is caused by the full admission from the second section. The simulation of an impeller uses the above described model without changes. The disadvantage of this model is based on assumption of fully mixed flows before they reach an impeller.

The layout of the current model with examples of velocity components is presented in Fig. 12. The model can be directly transferred to GT Power modules but the assumption of no vaneless space between impeller and position 12, i.e., $r_{12} = r_2$. The transformation of 2-D flow in vaneless nozzle to GT Power modules is under development.

An optional model would consist in conservation of separate flows until they reach the impeller inlet mixing of flows inside impeller. This model will be developed in future to compare the results. The reality may be between the both extreme models, of course.

Mass conservation between 12 – 2 with approximation from incompressible fluid corrected by C_m

$$\begin{aligned} \dot{m} &= 2\pi r b \rho c_r \\ r_2 b_2 \rho_2 c_{r2} &= r_{12} b_{12}^I \rho_{12}^I c_{r12}^I + r_{12} b_{12}^{II} \rho_{12}^{II} c_{r12}^{II} \\ c_{r2} &= \frac{r_{12}}{r_2 b_2} \frac{b_{12}^I \rho_{12}^I c_{r12}^I + b_{12}^{II} \rho_{12}^{II} c_{r12}^{II}}{\rho_2} = \frac{C_m r_{12}}{r_2 b_2} (b_{12}^I c_{r12}^I + b_{12}^{II} c_{r12}^{II}) = \frac{C_m r_{12}}{r_2 b_2} (b_{12}^I c_{12}^I \cos \alpha_{12}^I + b_{12}^{II} c_{12}^{II} \cos \alpha_{12}^{II}) \end{aligned} \quad (21)$$

C_m can be found, if densities – it means pressures and temperatures – are determined.

Let's assume for simplicity, that the pressure p_{12} is the future main unknown parameter, for which governing equation should be found. Then, energy conservation between 1 – 12 yields unknown inlet velocities - (23) and temperatures – see (27).

The case of rare but possible back-flow to the section with too low pressure has to be treated. The inlet velocity in unstreamed section is reversed, i.e., negative, determined approximately by static pressure in the mixing space, since the kinetic energy of streamed section may be fully dissipated if the flow is reversed. Since the velocity in unstreamed section is close to 0, total pressure and static pressure at the section inlet may be equal. This assumption might not be fully for vaneless nozzle, which would act in this case as a vaneless diffuser, but this case is too rare and too complicated to be treated in more details in this algebraic model.

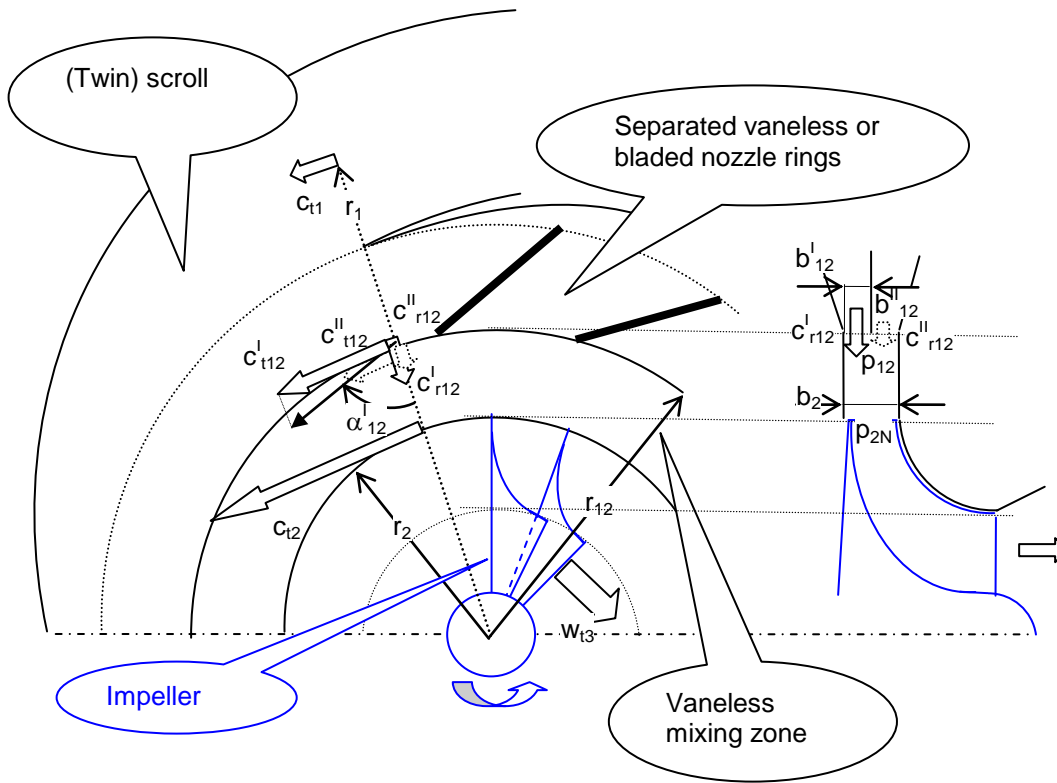


Fig. 12 Twin-scroll radial turbine layout

The mass flow-rate and energy equations for reversed flow must use not only negative sign of volumetric flow-rate but also upwind density or total enthalpy, i.e., those of flow inside gap **12**. The inlet total temperature is that of streamed section (i.e., cross exchanged between I and II). Upwind coefficients will help in writing generally valid relations using **sign** function

$$\begin{aligned} \gamma^{I,II} &= \frac{1 + \text{sign}(p_{01}^{I,II} - p_{12})}{2} = 1 \quad \text{for standard flow direction (state 01 upwind),} \\ \delta^{I,II} &= \frac{1 - \text{sign}(p_{01}^{I,II} - p_{12})}{2} = 1 \quad \text{for reversed flow direction (state 12 upwind)} \end{aligned} \quad (22)$$

Then, the velocities may be found with appropriate sign from Saint-Venant relations corrected to the losses by expansion efficiency and the volumetric flow-rate can be determined:

$$c_{12}^{I,II} = C_c^{I,II} \text{sign}(p_{01}^{I,II} - p_{12}) \sqrt{2\eta_N^{I,II} \frac{p_{01}^{I,II} - p_{12}}{\rho_{01}^{I,II}}}$$

$$C_c^{I,II} = \begin{cases} \text{if } |p_{01}^{I,II} - p_{12}| > 0 \text{ then } \gamma^{I,II} \frac{\sqrt{c_p T_{01}^{I,II} \left(1 - \left(\frac{p_{12}}{p_{01}^{I,II}}\right)^{\frac{\kappa-1}{\kappa}}\right)}}{\sqrt{\frac{p_{01}^{I,II} - p_{12}}{\rho_{01}^{I,II}}}} + \delta^{I,II} \frac{\sqrt{c_p T_{01}^{II,I} \frac{\eta_{Nb}^{I,II}}{\eta_N^{I,II}} \left(1 - \left(\frac{p_{01}^{I,II}}{p_{12}}\right)^{\frac{\kappa-1}{\kappa}}\right)}}{\sqrt{\frac{p_{12} - p_{01}^{I,II}}{\rho_{01}^{I,II}}}} \\ \text{else } 0 \end{cases} \quad (23)$$

$$\dot{V}^{I,II} = 2\pi r_{12} b_{12}^{I,II} \cos \alpha_{12}^{I,II} C_{12}^{I,II}$$

Mass flow-rates can be calculated from velocity with additional correction for compressibility and flow contraction with upwind density

$$\dot{m}^{I,II} = C_N^{I,II} \rho_{01}^{I,II} \dot{V}^{I,II} \quad (24)$$

Correction coefficients have not the same meaning here as C_N in (7) – it corrects only compressibility for density change and flow contraction. Moreover, sonic flow is treated only for the standard flow direction because the backward flow takes place at low pressure ratios only:

$$\dot{m}^{I,II} = \begin{cases} \text{if } \varepsilon^* = \left[1 - \frac{\kappa-1}{\eta_N^{I,II}(\kappa+1)}\right]^{\frac{\kappa}{\kappa-1}} < \frac{p_{2N}}{p_{01}} \text{ then} \\ \gamma^{I,II} \frac{(1 - K_{sep}^{I,II}) p_{01}^{I,II} \frac{p_{12}}{p_{01}^{I,II}}}{r T_{01}^{I,II} \left[1 - \eta_N^{I,II} \left[1 - \left(\frac{p_{12}}{p_{01}^{I,II}}\right)^{\frac{\kappa-1}{\kappa}}\right]\right]} \dot{V}^{I,II} + \delta^{I,II} \frac{(1 - K_{sep,b}^{I,II}) p_{12} \frac{p_{01}^{I,II}}{p_{12}}}{r T_{01}^{II,I} \left[1 - \eta_{Nb}^{I,II} \left[1 - \left(\frac{p_{01}^{I,II}}{p_{12}}\right)^{\frac{\kappa-1}{\kappa}}\right]\right]} \dot{V}^{I,II} \\ \text{else } 2\pi r_{12} b_{12}^{I,II} \cos \alpha_{12}^{I,II} \frac{p_{01}}{r T_{01}} \frac{\varepsilon^*}{1 - \eta \left[1 - \varepsilon^* \frac{\kappa-1}{\kappa}\right]} \sqrt{2r \frac{\kappa}{\kappa-1} T_{01} \eta_N \left[1 - \varepsilon^* \frac{\kappa-1}{\kappa}\right]} \end{cases} \quad (25)$$

$$C_N^{I,II} = \begin{cases} \text{if } |\dot{V}^{I,II}| > 0 \text{ then } \frac{\dot{m}_N^{I,II}}{\rho_{01}^{I,II} \dot{V}^{I,II}} \\ \text{else } 0 \end{cases} \quad (26)$$

Inlet temperatures can be found simply (excluding the case of backflow)

$$c_p(T_{01}^{I,II} - T_{12}^{I,II}) = \frac{c_{12}^{I,II2}}{2} = C_c^{I,II2} \eta_N^{I,II} \frac{\rho_{01}^{I,II} - \rho_{12}}{\rho_{01}^{I,II}}$$

$$T_{12}^{I,II} = \min\left(T_{01}^{I,II}, T_{01}^{I,II} - C_c^{I,II2} \eta_N^{I,II} \frac{\rho_{01}^{I,II} - \rho_{12}}{\rho_{01}^{I,II}}\right) \quad (27)$$

Unknown densities can be found from equation of state

$$\rho_{12}^{I,II} = \frac{\rho_{12}}{r T_{12}^{I,II}} \quad (28)$$

Up to now everything has been derived as a function of the pressure p_{12} .

Angular momentum conservation in the mixing zone – Fig. 12 – yields tangential component of the impeller inlet velocity

$$-r_{12}\left(\dot{m}' c_{t12}' + \dot{m}'' c_{t12}''\right) + r_2\left(\dot{m}' + \dot{m}''\right) c_{t2} = -M_f = -K_v r_2\left(\dot{m}' + \dot{m}''\right) c_{t2}$$

$$(1 + K_v) r_2\left(\dot{m}' + \dot{m}''\right) c_{t2} = r_{12}\left(\dot{m}' c_{t12}' + \dot{m}'' c_{t12}''\right) \quad (29)$$

which yields with approximation for incompressible fluid, corrected by C_t

$$c_{t2} = \frac{r_{12}\left(\dot{m}' c_{t12}' + \dot{m}'' c_{t12}''\right)}{(1 + K_v) r_2\left(\dot{m}' + \dot{m}''\right)} = \frac{r_{12}^2}{(1 + K_v) r_2^2 b_2} \frac{c_{r12}^I c_{t12}^I \rho_{12}^I b_{12}^I + c_{r12}^{II} c_{t12}^{II} \rho_{12}^{II} b_{12}^{II}}{c_{r2} \rho_2} =$$

$$= C_t \frac{r_{12}^2}{(1 + K_v) r_2^2 b_2} \frac{c_{r12}^I c_{t12}^I b_{12}^I + c_{r12}^{II} c_{t12}^{II} b_{12}^{II}}{c_{r2}} = \frac{C_t}{C_m} \frac{r_{12}}{(1 + K_v) r_2} \frac{c_{12}^{I2} \cos \alpha_{12}^I \sin \alpha_{12}^I b_{12}^I + c_{12}^{II2} \cos \alpha_{12}^{II} \sin \alpha_{12}^{II} b_{12}^{II}}{c_{12}^I \cos \alpha_{12}^I b_{12}^I + c_{12}^{II} \cos \alpha_{12}^{II} b_{12}^{II}} \approx$$

$$\approx \frac{C_t}{C_m} \frac{r_{12}}{(1 + K_v) r_2} \frac{c_{12}^{I2} + c_{12}^{II2}}{c_{12}^I + c_{12}^{II}} \sin \alpha_{12} \quad (30)$$

Last approximation is valid for the (approximately) same angles of scroll partition exits.

Radial momentum conservation between 12 – 1 yields pressures (Fig. 12). The pressure acts not only on cylindrical surfaces of the symmetric checking domain (between cylinders of r_{12} and r_2) but in general on oblique side walls of mixing space, as well. The radial pressure distribution and the averaged radius for area calculation is respected by tuning coefficient k_p . The averaged centrifugal force $F_{C,av}$ acts additionally on the flow.

$$\begin{aligned}
& -\dot{m}^I c_{r12}^I - \dot{m}^{II} c_{r12}^{II} + \left(\dot{m}^I + \dot{m}^{II} \right) c_{r2} = -2\pi r_2 b_2 p_{2N} + 2\pi r_{12} (b_{12}^I + b_{12}^{II}) p_{12} + \\
& + 2\pi (r_{12} + r_2) (b_2 - b_{12}^I - b_{12}^{II}) \frac{p_{2N} + p_{12}}{k_p} - F_{C,av} \\
& - r_{12} b_{12}^I c_{12}^{I2} \cos^2 \alpha_{12}^I - r_{12} b_{12}^{II} c_{12}^{II2} \cos^2 \alpha_{12}^{II} + r_{12} b_{12}^{II} K_R \left[\frac{C_m r_{12}}{r_2 b_2} (b_{12}^I c_{12}^I \cos \alpha_{12}^I + b_{12}^{II} c_{12}^{II} \cos \alpha_{12}^{II}) \right]^2 = \\
& = -r_2 b_2 p_{2N} + r_{12} (b_{12}^I + b_{12}^{II}) p_{12} + \\
& + (r_{12} + r_2) (b_2 - b_{12}^I - b_{12}^{II}) \frac{p_{2N} + p_{12}}{k_p} - \frac{F_{C,av}}{2\pi}
\end{aligned} \tag{31}$$

The centrifugal force is integrated approximately using averaged density and approximate conservation of angular momentum (tangential velocity from (30)) with correction coefficient K_C

$$\begin{aligned}
F_{C,av} &= \int_{r_2}^{r_{12}} 2\pi r b_{av} \rho_{av} \frac{c_t^2}{r} dr = \int_{r_2}^{r_{12}} 2\pi b_{av} \rho_{av} \frac{(c_{t2} r_2)^2}{r^2} dr = 2\pi b_{av} \rho_{av} (c_{t2} r_2)^2 \left(\frac{1}{r_2} - \frac{1}{r_{12}} \right) = \\
&= 2\pi K_C b_2 \rho_{2N} \left(\frac{C_t}{C_m} \frac{r_{12}}{(1 + K_v)} \frac{c_{12}^{I2} \cos \alpha_{12}^I \sin \alpha_{12}^I b_{12}^I + c_{12}^{II2} \cos \alpha_{12}^{II} \sin \alpha_{12}^{II} b_{12}^{II}}{c_{12}^I \cos \alpha_{12}^I b_{12}^I + c_{12}^{II} \cos \alpha_{12}^{II} b_{12}^{II}} \right)^2 \frac{r_{12} - r_2}{r_2} r_{12}
\end{aligned} \tag{32}$$

The both previous equations yield relation between pressures

$$\begin{aligned}
& -r_{12} b_{12}^I c_{12}^{I2} \cos^2 \alpha_{12}^I - r_{12} b_{12}^{II} c_{12}^{II2} \cos^2 \alpha_{12}^{II} + r_{12} b_{12}^{II} K_R \left[\frac{C_m r_{12}}{r_2 b_2} (b_{12}^I c_{12}^I \cos \alpha_{12}^I + b_{12}^{II} c_{12}^{II} \cos \alpha_{12}^{II}) \right]^2 + \\
& + K_C b_2 \rho_{2N} \left(\frac{C_t}{C_m} \frac{r_{12}}{(1 + K_v)} \frac{c_{12}^{I2} \cos \alpha_{12}^I \sin \alpha_{12}^I b_{12}^I + c_{12}^{II2} \cos \alpha_{12}^{II} \sin \alpha_{12}^{II} b_{12}^{II}}{c_{12}^I \cos \alpha_{12}^I b_{12}^I + c_{12}^{II} \cos \alpha_{12}^{II} b_{12}^{II}} \right)^2 \frac{r_{12} - r_2}{r_2} r_{12} = \\
& = \left[\frac{(r_{12} + r_2) (b_2 - b_{12}^I - b_{12}^{II})}{k_p} - r_2 b_2 \right] p_{2N} + \left[r_{12} (b_{12}^I + b_{12}^{II}) + \frac{(r_{12} + r_2) (b_2 - b_{12}^I - b_{12}^{II})}{k_p} \right] p_{12}
\end{aligned} \tag{33}$$

Impeller inlet pressure is then

$$\begin{aligned}
p_{2N} &= \frac{1}{\frac{(r_{12} + r_2) (b_2 - b_{12}^I - b_{12}^{II})}{k_p} - r_2 b_2} * \\
& * \left\{ \begin{aligned} & -r_{12} b_{12}^I c_{12}^{I2} \cos^2 \alpha_{12}^I - r_{12} b_{12}^{II} c_{12}^{II2} \cos^2 \alpha_{12}^{II} + r_{12} b_{12}^{II} K_R \left[\frac{C_m r_{12}}{r_2 b_2} (b_{12}^I c_{12}^I \cos \alpha_{12}^I + b_{12}^{II} c_{12}^{II} \cos \alpha_{12}^{II}) \right]^2 + \\ & + K_C b_2 \rho_{2N} \left(\frac{C_t}{C_m} \frac{r_{12}}{(1 + K_v)} \frac{c_{12}^{I2} \cos \alpha_{12}^I \sin \alpha_{12}^I b_{12}^I + c_{12}^{II2} \cos \alpha_{12}^{II} \sin \alpha_{12}^{II} b_{12}^{II}}{c_{12}^I \cos \alpha_{12}^I b_{12}^I + c_{12}^{II} \cos \alpha_{12}^{II} b_{12}^{II}} \right)^2 \frac{r_{12} - r_2}{r_2} r_{12} + \\ & - \left[r_{12} (b_{12}^I + b_{12}^{II}) + \frac{(r_{12} + r_2) (b_2 - b_{12}^I - b_{12}^{II})}{k_p} \right] p_{12} \end{aligned} \right\}
\end{aligned} \tag{34}$$

Now, we reduced three equations (one equation for mass and two equations for momentum conservation) from four unknowns - c_{r2} , c_{12} and p_{2N} – into single one for impeller inlet pressure p_{2N} as a function of unknown p_{12} , if energy conservation between 1 and 12 is used twice - (27) for sections outlet velocities and if for density (28) is used. Correction coefficients require determination of three densities at two pressures and three temperatures. The energy conservation between 12 and 2 completes the system for temperatures. The changes of temperature and composition are not significant, therefore enthalpy is integrated with $c_p = \text{const.}$ from $T_{ref} = 0K$.

$$\begin{aligned}
& -c_p \left(\dot{m}^I T_{01}^I + \dot{m}^{II} T_{01}^{II} \right) + \left(\dot{m}^I + \dot{m}^{II} \right) \left(c_p T_2 + \frac{c_{t2}^2 + c_{r2}^2}{2} \right) = 0 \\
T_{2N} &= \frac{\dot{m}^I T_{01}^I + \dot{m}^{II} T_{01}^{II}}{\dot{m}^I + \dot{m}^{II}} - \frac{c_{t2}^2 + c_{r2}^2}{2c_p}
\end{aligned} \tag{35}$$

which enables to find all correction coefficients if p_{12} is known.

Nevertheless, one equation is still missing. The pressure p_{2N} has to be found from the comparison of the mass flow-rate through nozzles and an impeller, see (4) or in more general form (20). For this purpose, it would be better to solve p_{12} as a function of p_{2N} to obtain single non-linear equation for p_{12} as a result. It is possible but really complicated because of square roots in relations between velocities and pressures.

This scheme may be directly transferred to GT Power objects, using mixing of enthalpies and momentum interaction in a general flow split . The only missing feature of a 1-D model is missing element with angular momentum conservation and different radius of inlet and outlet. For the current 1-D model the mixing is assumed to take part at fixed single radius and the flow is subjected after it to pass a nozzle with parameters equivalent to a vaneless nozzle.

The significant obstacle is created by the fact the procedure converges for deeply subsonic region only because of instabilities caused by correction coefficients.

New Turbine Modular Model with Pre-Defined Mass Flow-Rates

The amendment of the original turbine model (p. 5) combining it with twin-scroll description (p. 14) is in principle possible but too complicated for numerical solution. That is why completely new procedure was developed, reversing the coordinates for turbine mapping – instead of finding mass flow-rate and efficiency as a function of pressures at fixed speed and inlet total temperature(s), pressures and efficiency are found as a function of mass flow rates at fixed speed and (initially) fixed outlet temperature.

This approach made it possible that the whole procedure has been reversed, i.e., the exducer state creates starting for the numerical procedure, going upstream. It is not possible without iterations, of course, since at least inlet stagnation temperatures have to kept on fixed values. The outlet temperature has to be estimated to start upstream calculations. It is corrected at the end of procedure to inlet temperatures. Inlet stagnation pressures are the direct output of the numerical procedure. If fixed pressure ratio maps have to be found (unlike the case of standard turbine map measurement), another iteration to keep pressure ratio fixed is needed.

The backward going iteration is based on impeller total enthalpy conservation (including potential energy or rothalpy). Constant pressure thermal capacity is assumed to be independent on small temperature differences therefore reference temperature for zero enthalpy does not occur in the energy conservation equation. Now leakage along impeller blades is assumed (all leakage flow leaves the impeller blades upstream of an interblade channel). Then using known mass flow-rate and state downstream of impeller $p_{3I}, T_{3I}, \rho_3 = \frac{p_3}{rT_3}$

$$\begin{aligned}
 c_p T_{2I} + \frac{w_2^2}{2} - \frac{u_2^2}{2} &= c_p T_3 + \frac{w_3^2}{2} - \frac{u_3^2}{2} \\
 c_p T_3 k_T \left(\frac{T_{2I}}{T_3} \right) + \frac{1}{2} \left(\frac{\dot{m}_I}{A_{2I} \rho_3} \right)^2 \left(\frac{\rho_3}{\rho_{2I}} \right)^2 &= c_p T_3 + \frac{1}{2} \left(\frac{\dot{m}_I}{A_{3I} \rho_3} \right)^2 - \frac{u_3^2 - u_2^2}{2} \\
 c_p T_3 k_T \left(\frac{p_{2I}}{p_3} \right)^{\frac{\kappa-1}{\kappa}} + \frac{1}{2} \left(\frac{\dot{m}_I}{A_{2I} \rho_3} \right)^2 k_p \left(\frac{p_3}{p_{2I}} \right)^{\frac{2}{\kappa}} &= c_p T_3 + \frac{1}{2} \left(\frac{\dot{m}_I}{A_{3I} \rho_3} \right)^2 - \frac{u_3^2 - u_2^2}{2} = P \\
 c_p T_3 k_T x^{\frac{\kappa-1}{\kappa}} + \frac{1}{2} \left(\frac{\dot{m}_I}{A_{2I} \rho_3} \right)^2 k_p x^{\frac{2}{\kappa}} - P &= 0
 \end{aligned} \tag{36}$$

The last equation may be solved using Newton's method for unknown static pressure ratio

$$\begin{aligned}
 c_p T_3 k_T \left(\frac{p_{2I}}{p_3} \right)^{\frac{\kappa-1}{\kappa}} + \frac{1}{2} \left(\frac{\dot{m}_I}{A_{2I} \rho_3} \right)^2 k_p \left(\frac{p_3}{p_{2I}} \right)^{\frac{2}{\kappa}} &= P \\
 y &= K_1 x^{\frac{\kappa-1}{\kappa}} + K_2 x^{\frac{2}{\kappa}} - P \\
 \frac{dy}{dx} &= \frac{\kappa-1}{\kappa} K_1 x^{\frac{1}{\kappa}} - \frac{2}{\kappa} K_2 x^{\frac{2+\kappa}{\kappa}} \\
 x_{i+1} &= x_i - \frac{y_i}{\left(\frac{dy}{dx} \right)_i}
 \end{aligned} \tag{37}$$

The yet unknown correction coefficients have to be iterated since for the sake of simplicity they are not included into derivative. It is possible but since the iteration converges fast it is not needed. Moreover, as described below, there are other inevitable needs for iteration loops combined with basic Newton procedure. Using the definition of expansion efficiency and relations between stagnation or total and static states, the correction yields

$$\eta_I = \frac{\frac{w_3^2}{2}}{T_{rel02I} \left[1 - \left(\frac{p_3}{p_{rel02I}} \right)^{\frac{\kappa-1}{\kappa}} \right]} ; \quad \frac{T_0}{T} = \left(\frac{p_0}{p} \right)^{\frac{\kappa-1}{\kappa}}$$

$$k_T = \frac{\frac{T_{2I}}{T_3}}{\left(\frac{p_{2I}}{p_3} \right)^{\frac{\kappa-1}{\kappa}}} = \frac{\frac{T_{2I}}{T_{rel02I}} \frac{T_{rel02I}}{T_3}}{\left(\frac{p_{2I}}{p_3} \right)^{\frac{\kappa-1}{\kappa}}} = \frac{\left(\frac{p_3}{p_{rel02I}} \right)^{\frac{\kappa-1}{\kappa}}}{1 - \eta_I \left[1 - \left(\frac{p_3}{p_{rel02I}} \right)^{\frac{\kappa-1}{\kappa}} \right]} = \frac{\left(\frac{p_3}{p_{2I}} \right)^{\frac{\kappa-1}{\kappa}}}{1 - \eta_I \left[1 - \left(\frac{p_3}{p_{2I}} \right)^{\frac{\kappa-1}{\kappa}} \right]} \quad (38)$$

$$\frac{p_3}{p_{2I}} = \left(\frac{p_3}{p_{2I}} \right)^{\frac{1}{\kappa}} \frac{1}{k_T} \quad k_\rho = \left(\frac{1}{k_T} \right)^2$$

Taking into account that relative velocity at inlet to the interblade channel for a standard impeller is radial one and outlet velocity is defined by average angle of blades, the cross-section areas with a normal parallel to average flow direction corrected to blade thickness obstruction are

$$A_{3I} = \left[\pi(r_{3shroud}^2 - r_{3hub}^2) - z_{blades} b_{blade} (r_{3shroud} - r_{3hub}) \right] \cos \beta_3$$

$$A_{2I} = (2\pi r_{2I} - z_{blades,I} b_{blade,I}) b_{2I}$$

$$A_{2N}^{I \text{ or } II} = (2\pi r_{2N} - z_{blades,N} b_{blade,N}) b_{2N} \cos \alpha_{2N}^{I \text{ or } II} \quad (39)$$

Using this backward going procedure, all velocities and relative stagnation state variables can be simply found now at impeller inlet (i.e., after incidence loss took part). The incidence loss reference velocity needs not to be approximated as it was necessary in (11) - (13). Nevertheless, other iteration is needed since the relative tangential velocity before incidence loss takes part has to be found.

That is why the following procedure starts with scroll outlets mixing. The individual mass-flow rates and stagnation temperatures at scroll partition inlets are assumed to be fixed (and mutually different in general). The following relation without superscripts are applied for both scroll partitions

$$\left(\dot{m}^I + \dot{m}^{II} \right) c_p T_{02N} = \left[\dot{m}^I c_p T_{01}^I + \dot{m}^{II} c_p T_{01}^{II} \right]$$

$$T_{02N} = \frac{\dot{m}^I T_{01}^I + \dot{m}^{II} T_{01}^{II}}{\dot{m}^I + \dot{m}^{II}} \quad (40)$$

The scroll partitions outlet velocities can be found if static outlet pressure is known. Let's assume for a moment.

$$c_{2N}^i = \frac{\dot{m}^i}{A_{2N}^i \frac{p_{2N}}{r T_{2N}^i}} ; \quad c_p T_{01}^i = c_p T_{2N}^i + \frac{c_{2N}^{i2}}{2}$$

$$\frac{1}{2} \left(\frac{r \dot{m}^i}{A_{2N}^i p_{2N}} \right)^2 T_{2N}^{i2} + c_p T_{2N}^i - c_p T_{01}^i = 0 ; \quad T_{2N} = \frac{-c_p + \sqrt{c_p^2 + 2c_p T_{01} \left(\frac{r \dot{m}}{A_{2N} p_{2N}} \right)^2}}{\left(\frac{r \dot{m}_N}{A_{2N} p_{2N}} \right)^2} \quad (41)$$

Now partition outlet velocities and both tangential and radial components (using known exit angles) of them can be found. If immediate mixing is assumed at radius of scroll partitions outlet with no pressure change (it can be corrected by calibration coefficient K_m). The momentum conservation yields

$$c_{r2N} = \left(\frac{\dot{m}^I}{\dot{m}^I + \dot{m}^{II}} c_{r2N}^I + \frac{\dot{m}^{II}}{\dot{m}^I + \dot{m}^{II}} c_{r2N}^{II} \right) K_m = w_{r2N}$$

$$c_{t2N} = \frac{\dot{m}^I}{\dot{m}^I + \dot{m}^{II}} c_{r2N}^I \tan \alpha_2^I + \frac{\dot{m}^{II}}{\dot{m}^I + \dot{m}^{II}} c_{r2N}^{II} \tan \alpha_2^{II} \quad (42)$$

Using known velocity components, the incidence angle relative to impeller blades can be found. The difference between radial relative velocity in impeller before and after the incidence loss can be respected by changing radial velocity (due to density difference and possible area reduction) without any change of relative tangential one

$$\zeta_{I,inc} = 2 \frac{p_{rel/02N} - p_{rel/02I}}{\rho_{2I} w_{2I}^2} = (\tan \beta_2 + K_{imp})^2 = \left(\tan \alpha_{2I} - \frac{u_2}{w_{2I}} + K_{imp} \right)^2 = \left(\frac{c_{t2N} - u_2}{w_{2I}} + K_{imp} \right)^2 \quad (43)$$

Then knowing relative stagnation pressure at impeller inlet after incidence loss, the previous relation yields

$$p_{rel/02N} = p_{rel/02I} + \zeta_{I,inc} \rho_{2I} w_{2I}^2 \quad (44)$$

and static pressure and temperature at relative flow for impeller before incidence loss occurs can be found

$$T_{rel/0N} = T_{rel/0I} = T_{2I} + \frac{w_{2I}^2}{2c_p} ; \quad T_{2N} = T_{rel/0N} - \frac{(c_{t2N} - u_2)^2}{2c_p}$$

$$p_{2N} = p_{rel/02N} \left(\frac{T_{2N}}{T_{rel/02}} \right)^{\frac{\kappa}{\kappa-1}} \quad (45)$$

Knowing the state parameters in the gap between a nozzle ring and an impeller, leakages at both shroud side and the impeller disk (hub side) may be found. The experience from previous simulations has shown that both flows under influence of centrifugal force (part of a shroud side) and without it (just a nozzle flow) should be respected, the cross sections being calibration parameters. Without these flows, the calibration of model may be impossible since the kinetic energy losses influence both flow-rates and efficiency in one direction (high losses – low flow-rate and poor efficiency), while leakage increases flow-rate with simultaneous reduction of efficiency.

$$\dot{m}_I = \dot{m}^I + \dot{m}^{II} - \Delta \dot{m}_{leakage} \quad (46)$$

As a result, we have now two relations for T_{2N} , namely (45) and (41). However, the latter one was deduced with assumption of exducer exit temperature T_3 . The difference between those results has to be used for correction of T_3 .

This creates the last iteration, which should be done after all partial iteration have been converged. If it is combined in the single iteration loop, the danger of divergence is quite high. It can be amended by another Newton solver (with numerically found derivative) but even in this case the convergence is not good for very different mass flows or at very low or high turbine speed with significant incidence losses.

At the end of the whole cycle, the definition of expansion efficiency is used for finding total pressure at partition inlet from pressure at partition outlet

$$\eta_N = \frac{\frac{c_{2N}^2}{2}}{T_{01} \left[1 - \left(\frac{p_{2N}}{p_{01}} \right)^{\frac{\kappa-1}{\kappa}} \right]} ; \quad p_{01} = \frac{p_{2N}}{\left(1 + \frac{c_{2N}^2}{2\eta_N T_{01}} \right)^{\frac{\kappa}{\kappa-1}}} \quad (47)$$

Before the turbine power is calculated, windage losses of an impeller should be deduced from the total head obtained in expansion. Thus the last tuning coefficient K_{vent} is defined

$$\Delta h_{vent} = \frac{K_{vent} \rho_{2N} D_{2I}^2 u_2^3}{\dot{m}_T \text{Re}^{0.2}}, \quad \text{Re} = \frac{u_2 D_{2I}}{\nu_{2N}} \quad (48)$$

Then, turbine power can be found from mass flow-rate and specific power, usually from both Stodola (difference of total enthalpies) or Euler (angular momentum conservation) equations using parameters at impeller inlet and exit in absolute (i.e., fixed in space) coordinate system – see (2). The differences between them check the accuracy of numerical procedure and according to the experience are less than 1%.

The outlined procedure has to be completed by the treatment of possible transonic flows, limiting the velocities to sonic ones and changing accordingly pressure ratios, and by the backflow conditions for very high centrifugal forces. In the future, the additional vaneless nozzle - (75) - (81), already involved in GT Power model, will be added between scroll partitions exits and an impeller. The model may take into account the friction torque loss as described in mentioned relations.

The model is important for understanding the additional has been used for the assessment of all losses due to partial admission using twin scroll. The further results were found using it with calibration extrapolated for single scroll turbine of large trim.

Before those results are presented, the definitions of turbine map parameters have to be stated.

Turbine Map Parameters

Enthalpy Head at a Turbine

Enthalpy head enables the calculation of turbine power. It is possible using the Euler equation or a total enthalpy head (both approaches are recommended to be compared in the current procedure to be sure that iterations work properly). Then the usable enthalpy head and turbine power is obviously for a single scroll turbine

$$\begin{aligned}\pi_T &= \frac{p_{01}}{p_3}; \quad c_s = \sqrt{2c_p T_{01} \left(1 - \pi_T^{\frac{1-\kappa}{\kappa}}\right)}; \quad x = \frac{u_2}{c_s} \\ c_T &= \sqrt{2\Delta h_T} = \sqrt{2(u_2 c_{t2N} - u_3 c_{t3} - \Delta h_{vent}) \frac{\dot{m}_I}{\dot{m}_N}} \\ P_T &= \dot{m}_N \frac{c_T^2}{2} \\ \eta_{Ts} &= \frac{c_T^2}{c_s^2}\end{aligned} \quad (49)$$

A reduction of leakage influence is involved. An ideal expansion velocity c_s and - for comparison - the apparent one c_T provide information for the isentropic efficiency and the blade tip velocity ratio x .

If a twin-scroll is used, the real turbine parameters are changed in an expected way

$$\begin{aligned}c_T &= \sqrt{2\Delta h_T} = \sqrt{2(u_2 c_{t2N} - u_3 c_{t3} - \Delta h_{vent}) \frac{\dot{m}_I}{\dot{m}^I + \dot{m}^{II}}} \\ P_T &= \left(\dot{m}^I + \dot{m}^{II}\right) \frac{c_T^2}{2}\end{aligned} \quad (50)$$

The issue is created by parameters of ideal turbine since they do not exist and have to be defined. Enthalpy head can be averaged using weighting by mass flow-rate in a very natural way.

$$\begin{aligned}\pi_T^i &= \frac{p_{01}^i}{p_3}; \quad c_s^i = \sqrt{2c_p T_{01}^i \left(1 - \pi_T^{i\frac{1-\kappa}{\kappa}}\right)}; \quad x^i = \frac{u_2}{c_s^i} \\ c_s &= \sqrt{\frac{c_s^{I2} \dot{m}^I + c_s^{II2} \dot{m}^{II}}{\dot{m}^I + \dot{m}^{II}}}\end{aligned} \quad (51)$$

There is no simple procedure for averaging of pressure ratio. Approximately it can be weighted by mass flow-rate, as well, since the pressure difference creates the significant part of enthalpy head

$$\pi_T \approx \frac{\pi_T^I \dot{m}^I + \pi_T^{II} \dot{m}^{II}}{\dot{m}^I + \dot{m}^{II}} \quad (52)$$

More accurate procedure is averaging according to the enthalpy head, mass flow rate and total inlet temperature after mixing, i.e

$$2c_p T_{02} \left(1 - \pi_T^{\frac{1-\kappa}{\kappa}} \right) \left(\dot{m}^I + \dot{m}^{II} \right) = c_s^{I^2} \dot{m}^I + c_s^{II^2} \dot{m}^{II}$$

$$\pi_T = \left(1 - \frac{c_s^{I^2} \dot{m}^I + c_s^{II^2} \dot{m}^{II}}{2c_p T_{02} \left(\dot{m}^I + \dot{m}^{II} \right)} \right)^{\frac{\kappa}{1-\kappa}} \quad (53)$$

The numerical exercise shows that bot averaging are not very different, the difference not exceeding 5%. However, even this averaging is not decisive for mass flow-rate influence since the density change, significant at high pressure ratio, is not taken into account.

For the mass flow-rate averaged pressure ratio, Saint-Venant-Wantzel equation is not suitable, since it cannot be solved for pressure ratio in closed form. The approximation by incompressible fluid flow yields

$$\dot{m} = A_{ref} \sqrt{2 \frac{p_{T2}^2}{rT} (\pi_T - 1)}$$

$$\pi_T = 1 + \frac{rT}{2p_{T2}^2 A_{ref}^2} \dot{m}^2 \quad (54)$$

It is much better to express the maps for partial admission as separated maps for both sections of a turbine with local pressure ratio and mass flow-rate. It should be stressed here that the maps are used in this case to demonstrate the changed turbine features and contribute thus to better understanding the complicated matter only, not to define the turbine features for GT Power and interpolate between them (FEV approach). The GT Power input is in the case of 1-D modelling based on detailed modular model, which adds the power delivered by sections in appropriate physically accurate location, not at upstream a turbine using inappropriate pressures.

Other CRT Performance Parameters

Pressure ratio π_T and blade-speed ratio BSR ... x (49) are the sole independent parameters for turbine characteristics presentation. As dependent ones a discharge coefficient μ_T and isentropic efficiency η_{Ts} are used. The discharge coefficient is used for a versatile presentation of turbine flow-rate capacity. A pure geometric definition of a reference area A_{Tref} is not obvious at a CRT. In the current report, the reference area is chosen in such a way that for the pressure ratio $\pi_T = 2$ is $\mu_T = 1$. The flow function ψ is a standard one for a compressible isentropic flow according to (73), changing to constant if the isentropic critical pressure ratio is achieved. Turbine isentropic efficiency is defined with correction to all aerodynamic losses caused by impeller leakage and windage of its disc.

Mechanical losses in bearings are not described in the current reprot although they can be modeled simply using generalized results of turbine characteristics measurement, too. Finally, a kinematic reaction of a turbine r_k is calculated, which is significant for comparison with detailed test results:

$$\dot{m}_{ref} = A_{Tref} \frac{p_{01}}{\sqrt{rT_{01}}} \sqrt{\psi} ,$$

$$\mu_T = \frac{\dot{m}_T}{\dot{m}_{ref}} ; \quad \eta_{Ts} = \left(\frac{c_T}{c_s} \right)^2 ; \quad (55)$$

$$r_k = 1 - \frac{c_{2N}^2 - c_3^2}{2(u_2 c_{t2N} - u_3 c_{t3})} .$$

The pressure-dependent function of ψ is defined in (73) with the turbine reciprocal pressure ratio from (72), $\varepsilon = 1/\pi_T$.

The preliminary optimization of a turbine impeller shape depends on a non-dimensional specific speed (well-known from water turbines and pumps)

$$n_{spec} = n_T \frac{\sqrt{\dot{m}_T / \rho_1}}{\sqrt[4]{c_s^6 / 8}} \quad (56)$$

which is calculated as another dependent performance parameter.

Tuning Parameters

In the simpler case without a twin-entry nozzle ring, the model features the following 9 tuning parameters: flow exit angles α_2 (or K_{v1} in the case of a vaneless nozzle – (79)), β_3 , the expansion efficiencies of kinetic velocity transformation η_N , η_h , incidence loss correction K_{inc} , impeller outlet reduction due to separated flow $K_{l\ sep}$, discharge coefficients of leakages $K_{leak\ seal}$, $K_{leak\ shroud}$ and windage loss coefficient K_{vent} . In the case of a twin-scroll turbine the expansion efficiencies and exit angles are separately determined for both partitions of a scroll (especially if non-symmetrical scroll is used). The momentum mixing correction coefficient K_m becomes the last parameter.

Supplementing only those geometry data of a turbine that can be easily measured (i.e. linear dimensions, diameters etc.) the model is ready for simulation provided that the tuning parameters are evaluated from tests.

Examples of the First Results

This part presents the first results of model calibrated for uniform admission to both partitions of a twin scroll and subjected to two different levels of partial admission, namely 50% in the other partition or small fixed mass flow-rate in it. The maps are presented here as a tool for better understanding of turbine parameters, not as maps suitable for 1-D code input since the philosophy of 1-D modelling is based on detail representation of a turbine elements.

Both SAE maps at fixed reduced speed and dimensionless BSR curves at almost fixed pressure ratio (suitable., e.g., for GT Power normalization procedure or for direct regression input to GT Power) are shown in the pictures below.

Pressure ratio used for SAE maps is calculated for energy-averaged incompressible flow according to (52). Except for the last case at extremely high pressure ratio all reduced mass flow curves converge to the same limit - Fig. 13. The high pressure ratio (close to 4) case is not accurate due to insufficient treatment of transonic flow through nozzle ring. This issue will be treated in the next version of a code.

The isentropic efficiency has been determined for total states upstream and static pressure downstream of a turbine, while power averaged isentropic power has been used for partial admission. The efficiency presented is internal one, i.e., windage losses have to be added for the total efficiency (reduction in average by 1 – 2% points, dependent on speed). The same weighting for averaging has been used for averaged BSR in Fig. 14. The efficiency map is typical for a too large trim of turbine with too small exducer (limited by design features of turbine shroud), namely the efficiency goes down starting with quite small pressure ratio due to overloaded exducer if density ratio becomes too large, causing large velocity and kinetic energy loss at outlet. The efficiency predicted for the largest pressure ratio suffers the same errors as flow-rate does as described above. The parameters are consistent with measurements.

The influence of partial admission is presented in Fig. 15 - Fig. 18 for the same couples of parameters. Although the mixing of flows with different momentum at nozzle outlets brings additional loss of kinetic energy at impeller inlet, the reduction of mass flow-rate through impeller unloads an exducer and changes significantly the efficiency dependence on pressure ratio - Fig. 15. The further increase of asymmetry in admission stresses this trend, although the maximum efficiency is reduced in the manner similar to closed VGT nozzle (rack position 0) - Fig. 17. The strange behavior of curves at low pressure ratios and high speed (far from efficiency optimum) is caused by only preliminarily treated back flows in a turbine. The current model sets just zero flow-rate for the in reality backflow. Both those errors are already treated in GT Power 1-D model. On the other hand, the errors of the highest pressure ratio at uniform admission are insignificant during partial admission due to the overall reduction of flow-rate through the exducer.

These features call for appropriate optimization of turbines for high pulsation factor, as it is used for twin-scroll four cylinder engine turbochargers (two cylinders with 360° distance between pulses). The results of turbine matching should be used in turbine design. The force of the model created is especially in this transfer of turbine features found during mapping back to the design stage at a turbocharger manufacturer. The model itself is not fully predictive, using experimentally or in CFD found loss coefficient but it is suitable for extrapolation before detailed CFD simulation or experiments are done.

The support of those results can be found in dimensionless maps for the cases described above in Fig. 19 - Fig. 24. The change of turbine reaction at reduced mass flow-rates shifts the optimum BSR towards lower values if partial admission is applied. The turbine discharge coefficient, correcting ideal nozzle flow of fixed reference cross section area to the real turbine flow, has been calculated for nozzle flow with flow-rate averaged pressure ratio - (54) - unlike the power averaged pressure ratio used in previous SAE maps.

Due to very high non-linearity of mass flow-rate as a function of pressure ratio (or pressure difference, which can be found from π_T at fixed outlet pressure using linear transform) the mass flow-rate for partial admission is very different from the reference nozzle and the discharge coefficient becomes much greater than one. It illustrates once again that those maps have limited use for lumped parameters modelling of a turbocharger. Nevertheless, they can be combined with the current GT Power approach, in which interpolation between two independent flow-rate maps for partitions of a scroll are used. Those partition flow-rate maps can be produced by the current twin scroll model, as well, if necessary. However, the basic issue consists in the fact that the flow between partitions is governed by internal turbine pressure not simply depending on the overall pressure ratio.

Therefore, the full 1-D model with internal mixing after the partial expansion in both scroll partitions works much better.

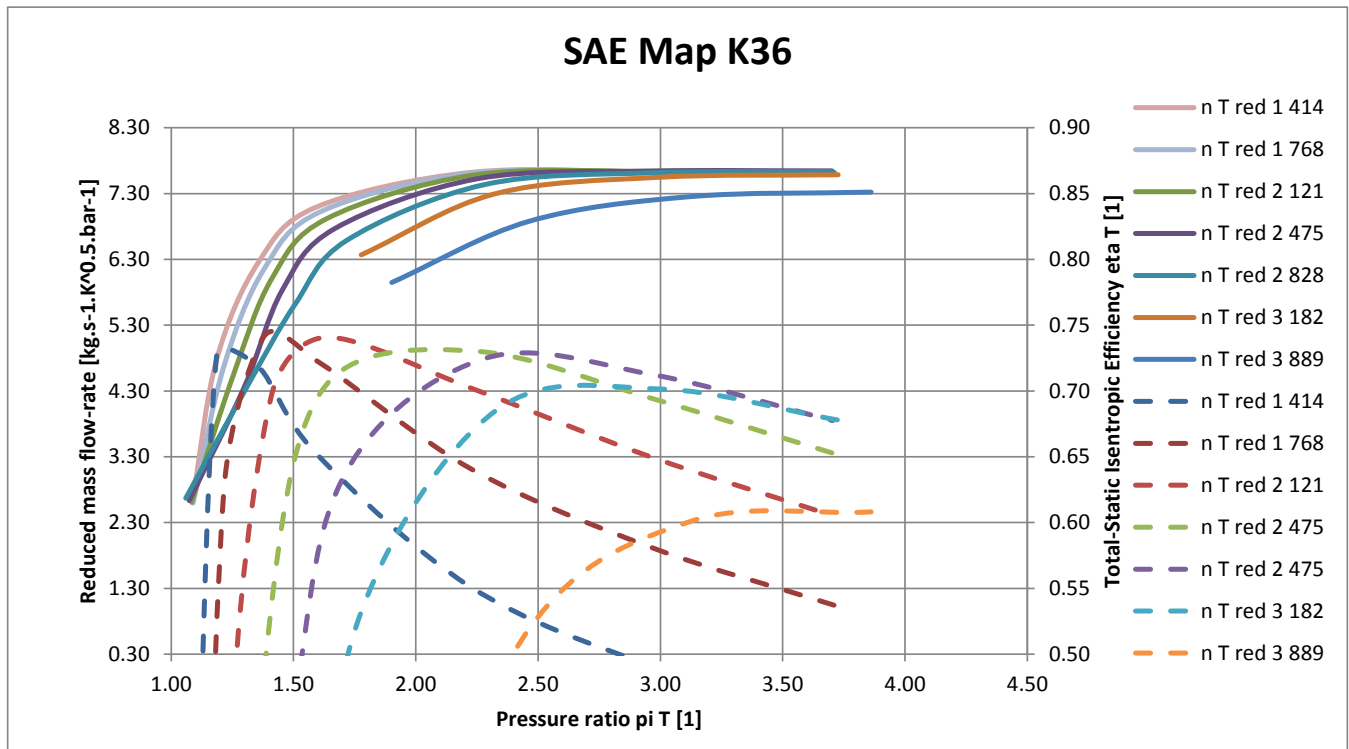


Fig. 13 Predicted map of CZ K36 turbine – the largest trim (model calibrated by experiments). Reduced mass flow-rate and internal total-to-static isentropic efficiency at full admission to a twin scroll

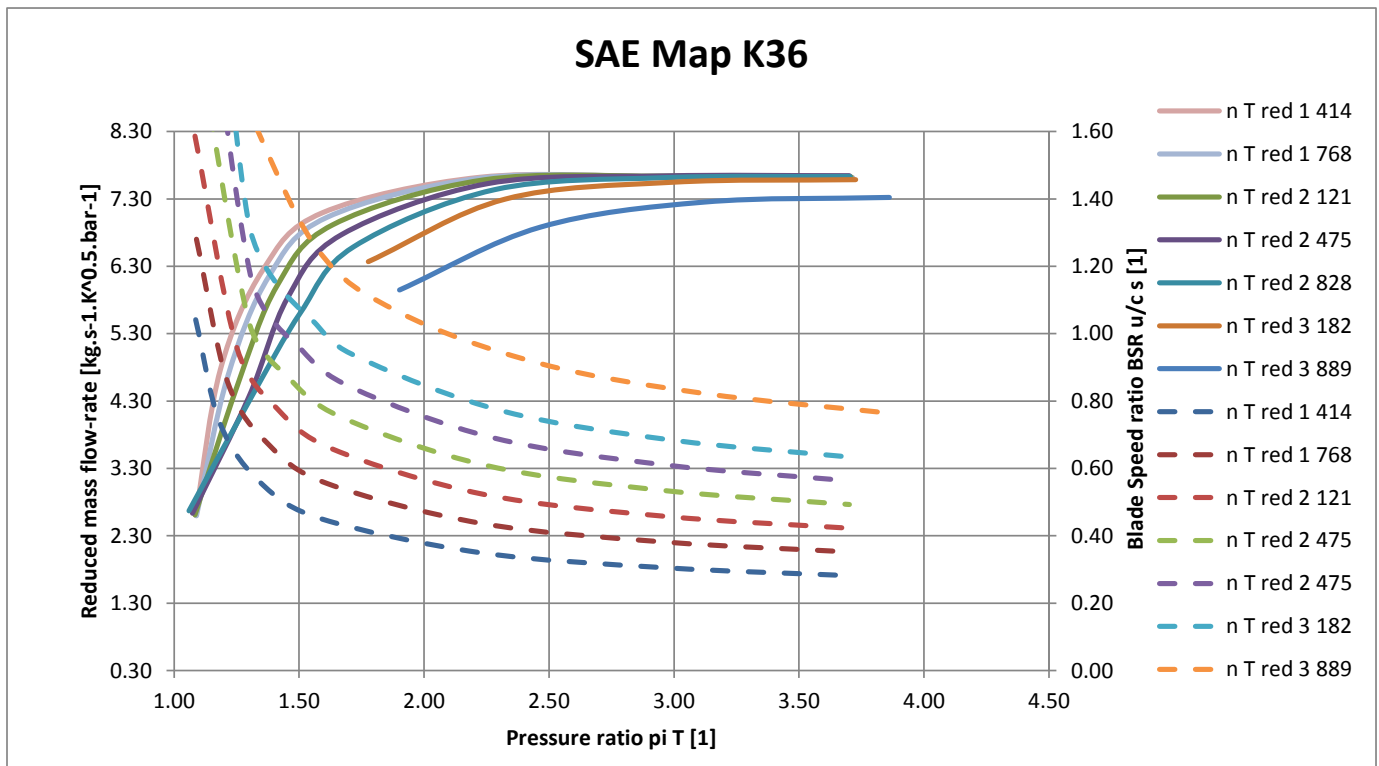


Fig. 14 Predicted map of CZ K36 turbine – the largest trim (model calibrated by experiments). Reduced mass flow-rate and BSR at full admission to a twin scroll

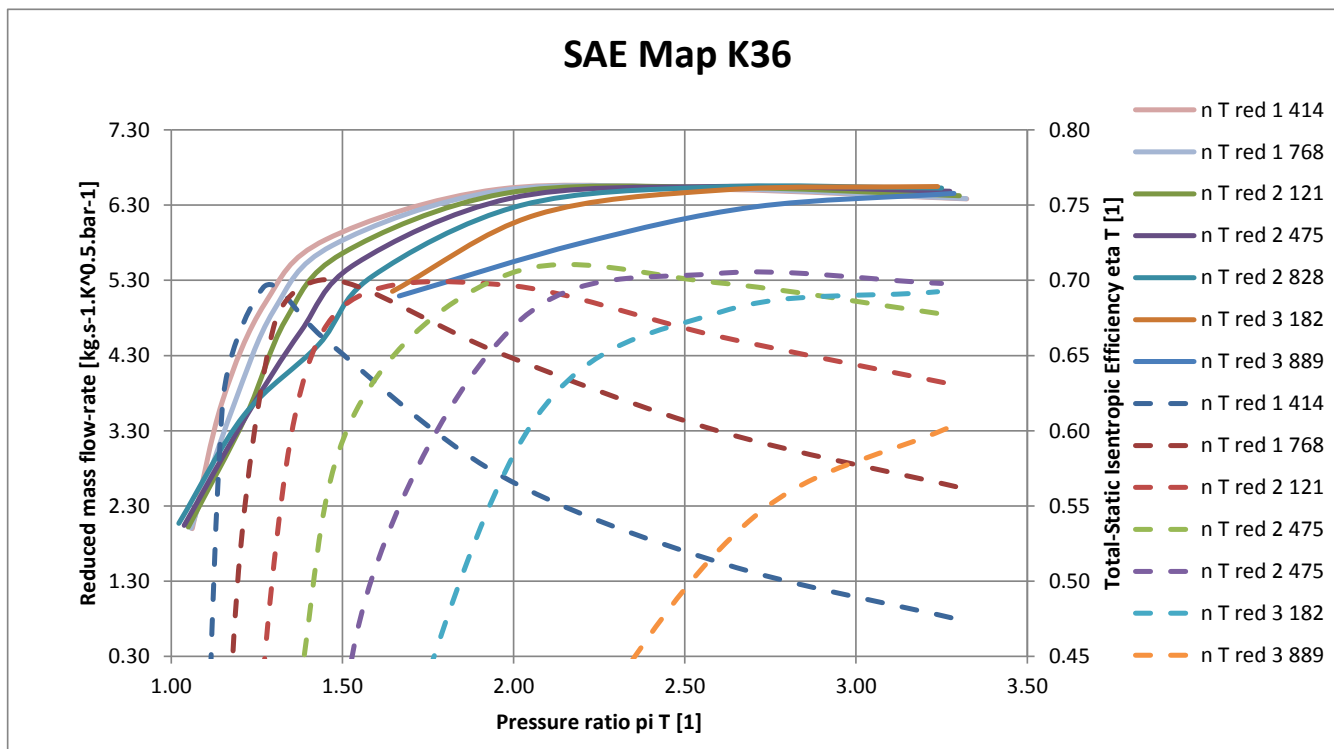


Fig. 15 Predicted map of CZ K36 turbine – the largest trim for 50% admission in the second partition of a twin scroll. Reduced mass flow-rate and internal total-to-static isentropic efficiency

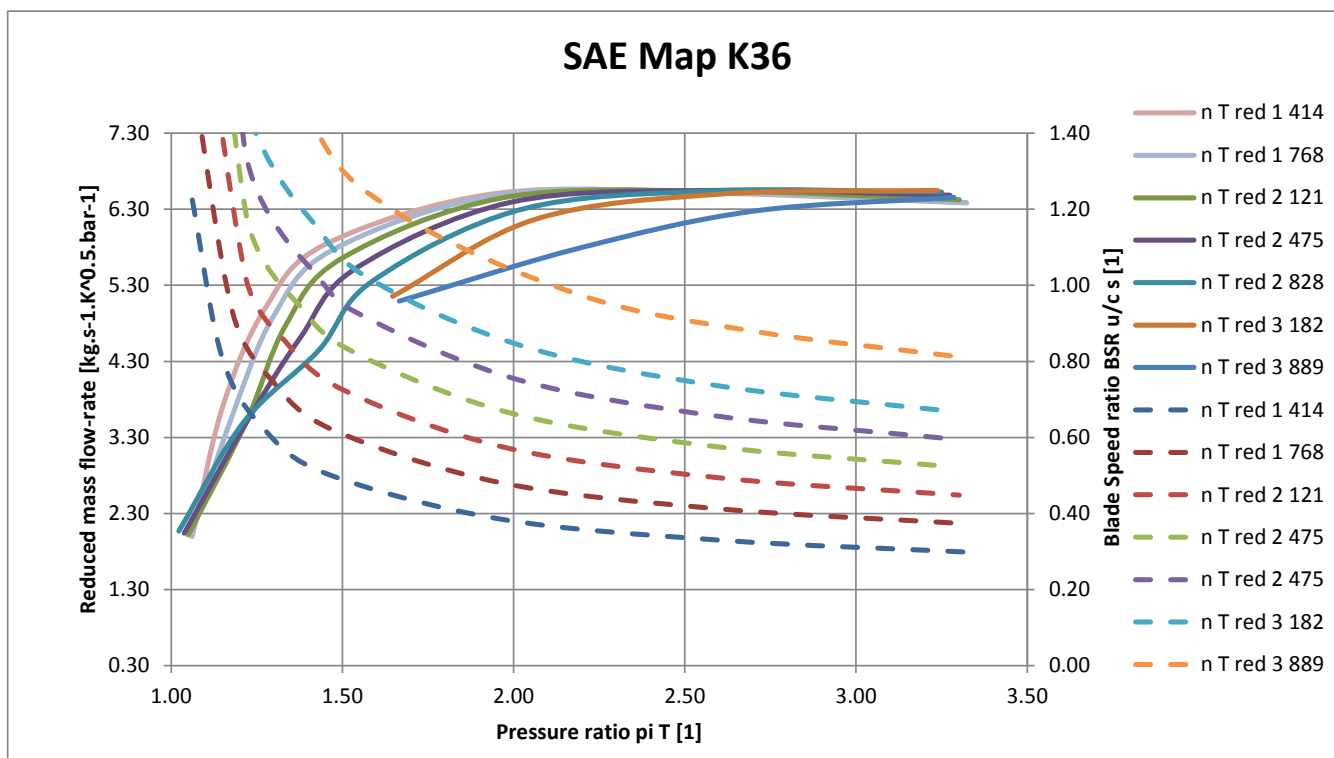


Fig. 16 Predicted map of CZ K36 turbine – the largest trim for 50% admission in the second partition of a twin scroll. Reduced mass flow-rate and BSR

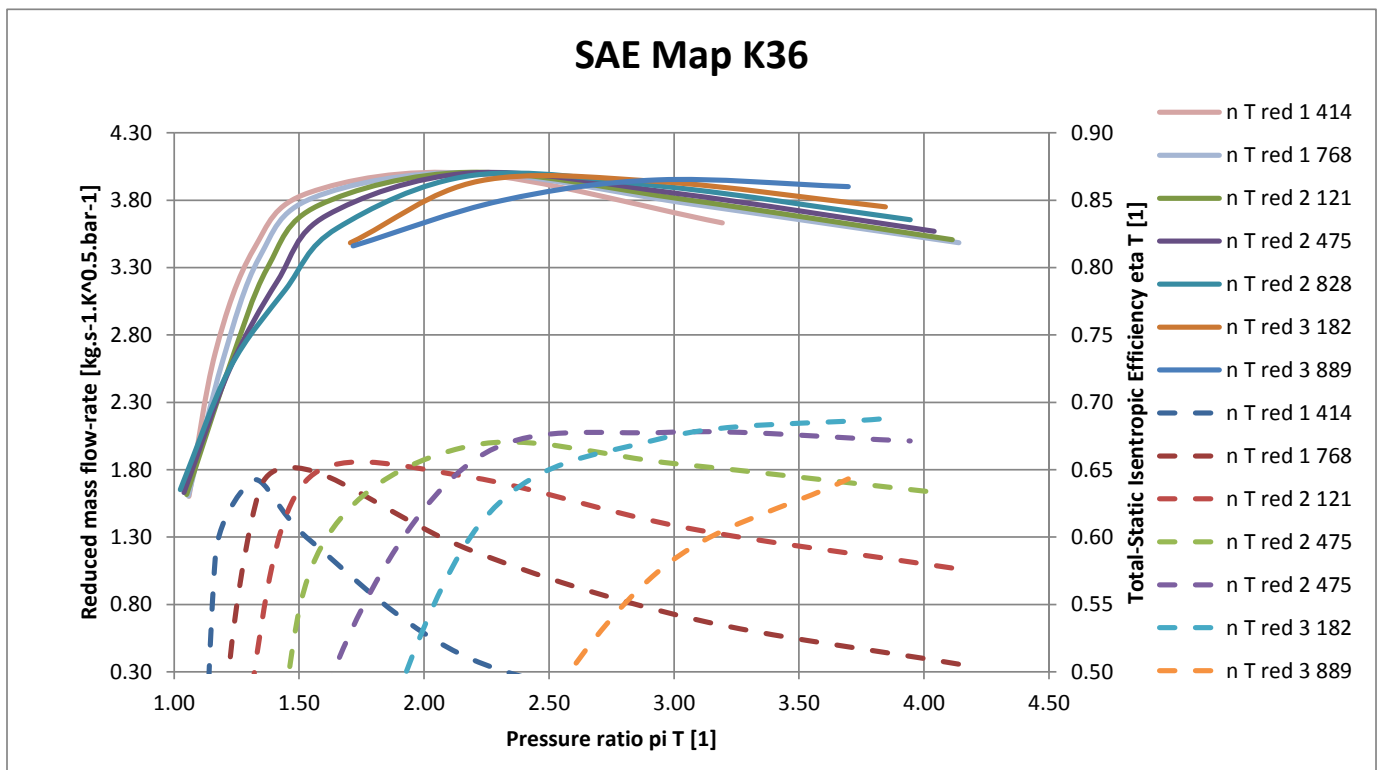


Fig. 17 Predicted map of CZ K36 turbine – the largest trim for fixed $0.01 \text{ kg} \cdot \text{s}^{-1}$ (approx. averaged reduced mass flow-rate of $0.26 \text{ kg} \cdot \text{s}^{-1} \cdot \text{K}^{0.5} \cdot \text{bar}^{-1}$) admission in the second partition of a twin scroll. Reduced mass flow-rate and internal total-to-static isentropic efficiency

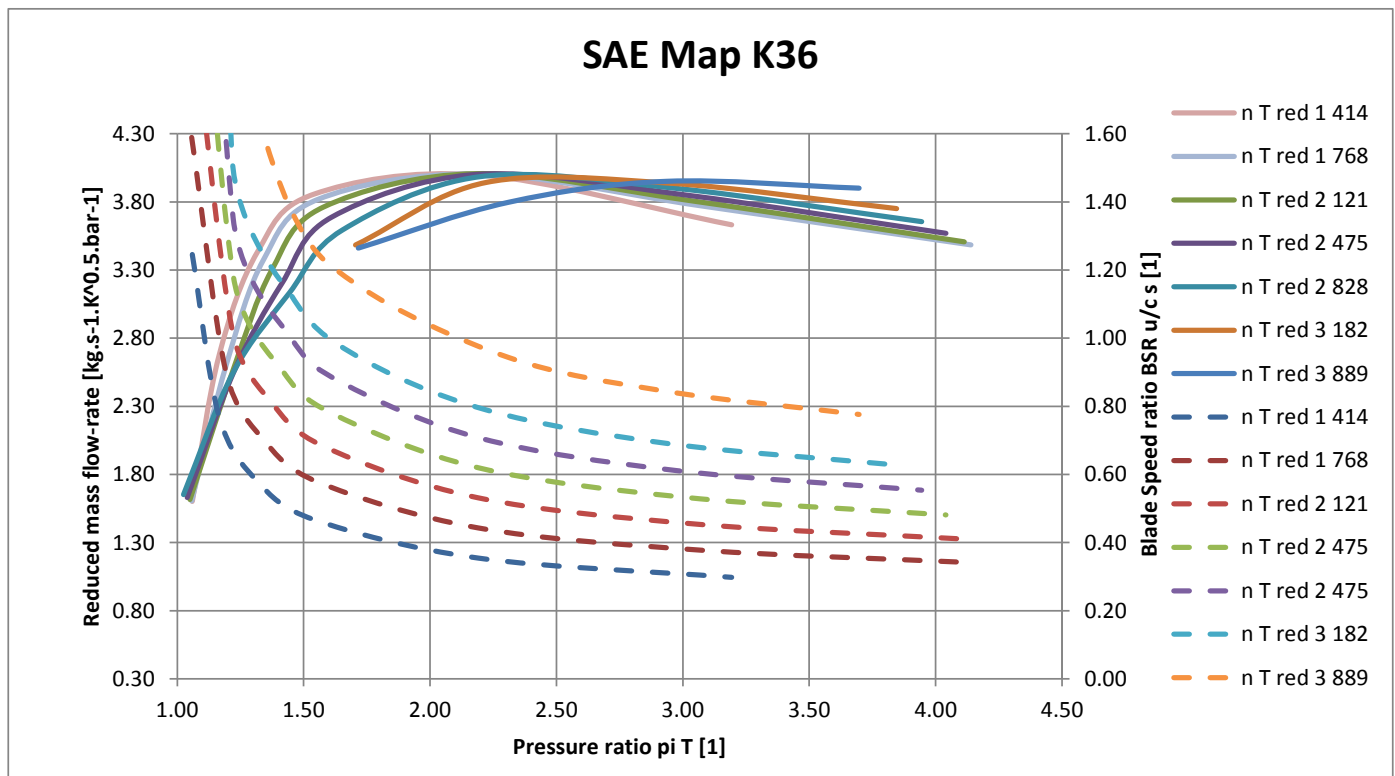


Fig. 18 Predicted map of CZ K36 turbine – the largest trim for fixed $0.01 \text{ kg} \cdot \text{s}^{-1}$ (approx. averaged reduced mass flow-rate of $0.26 \text{ kg} \cdot \text{s}^{-1} \cdot \text{K}^{0.5} \cdot \text{bar}^{-1}$) admission in the second partition of a twin scroll. Reduced mass flow-rate and total-to-static isentropic efficiency

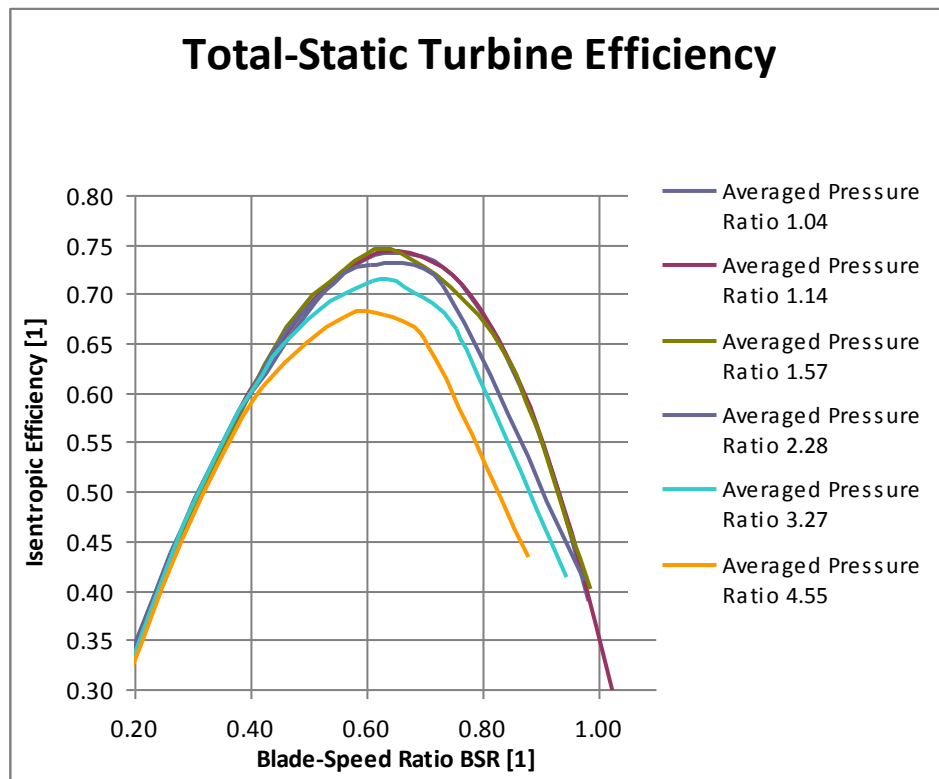


Fig. 19 Predicted BSR dependence of internal total-to-static isentropic efficiency for CZ K36 turbine – the largest trim (model calibrated by experiments) at full admission to a twin scroll

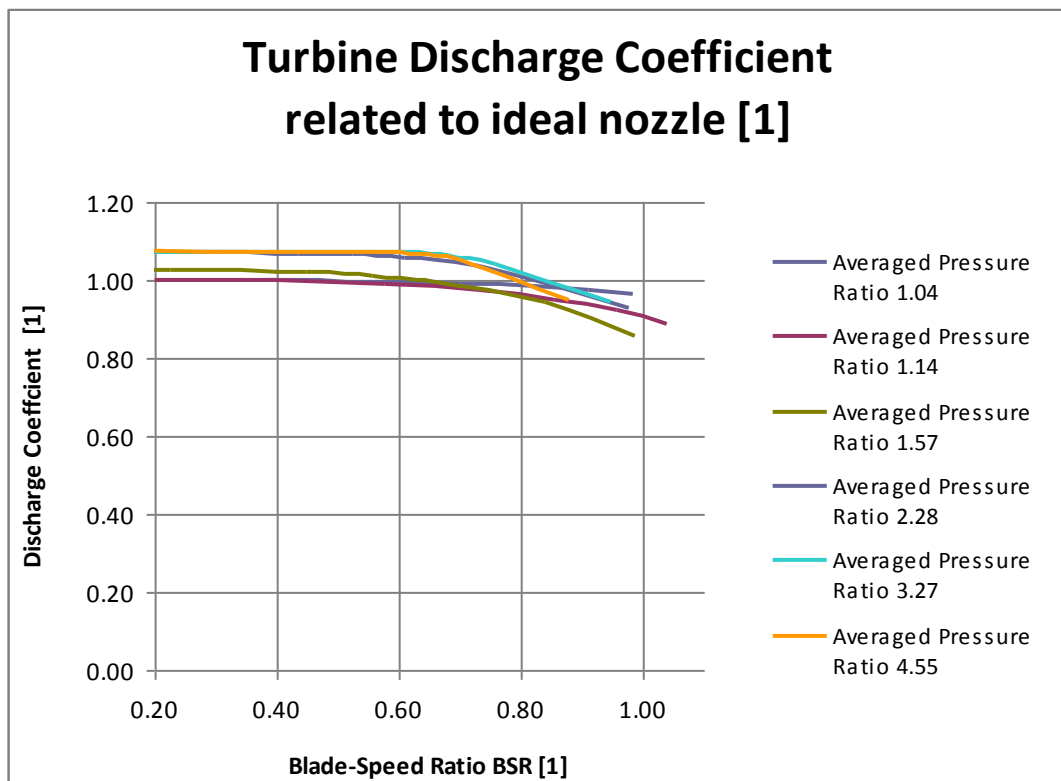


Fig. 20 Predicted BSR dependence of discharge coefficient for CZ K36 turbine – the largest trim (model calibrated by experiments) at full admission to a twin scroll. Reference cross-section area of 18 cm²

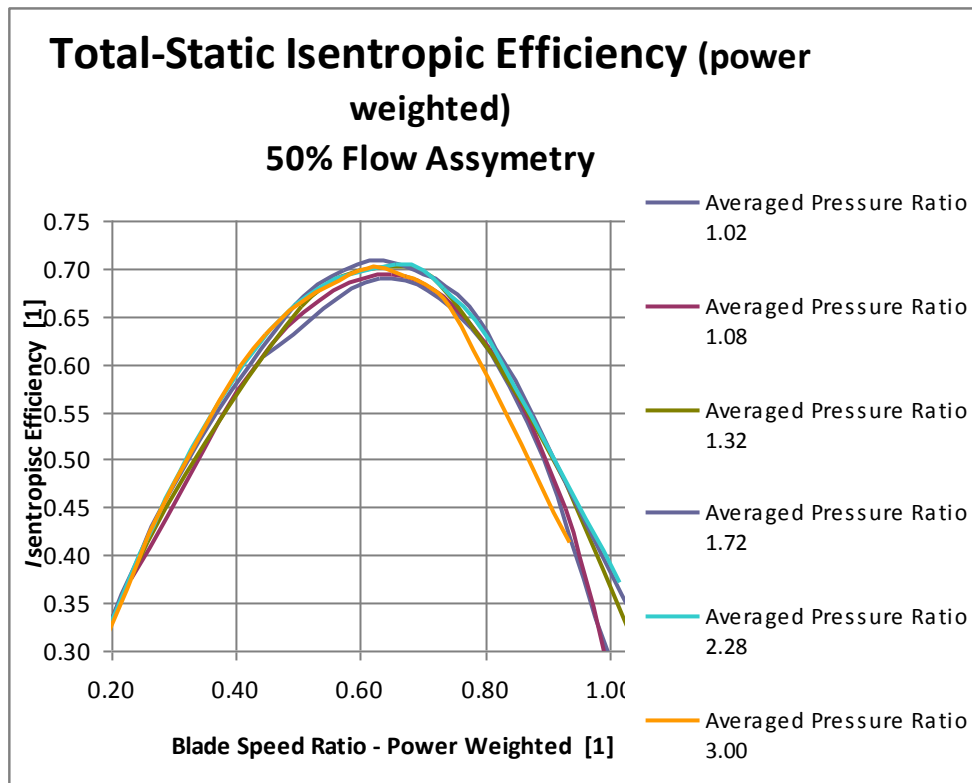


Fig. 21 Predicted BSR dependence of internal total-to-static isentropic efficiency of CZ K36 turbine – the largest trim for 50% admission in the second partition of a twin scroll

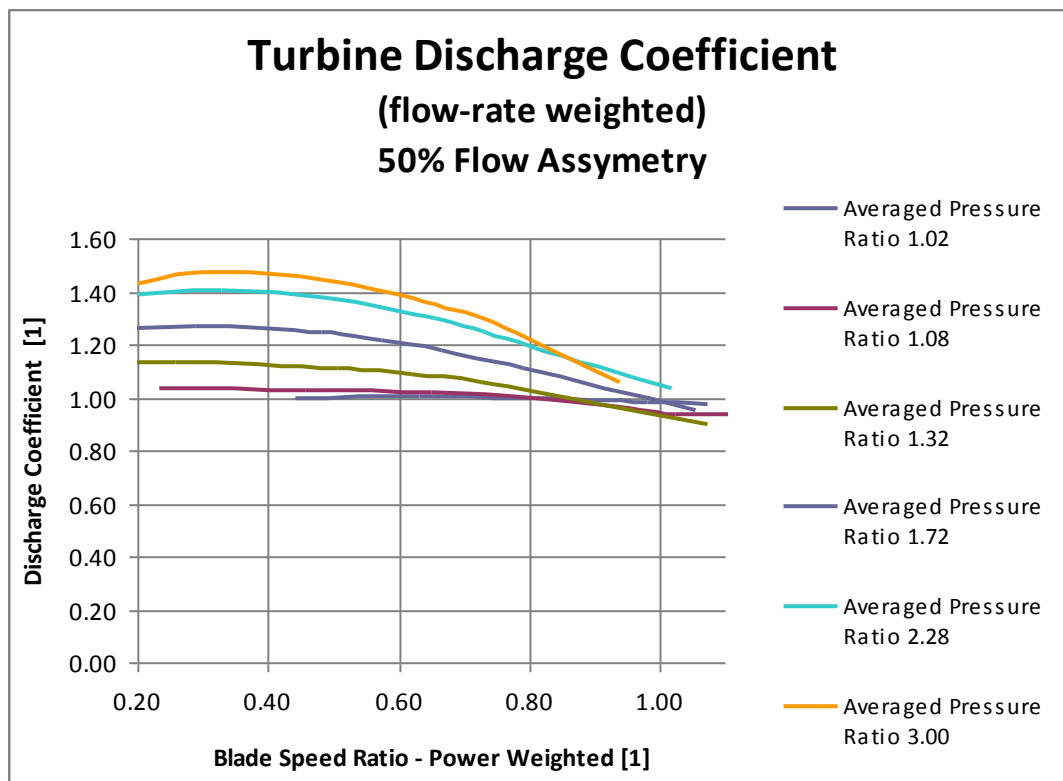


Fig. 22 Predicted BSR dependence of discharge coefficient for CZ K36 turbine – the largest trim (model calibrated by experiments) at 50% admission in the second partition of a twin scroll. Reference cross-section area of 18 cm²

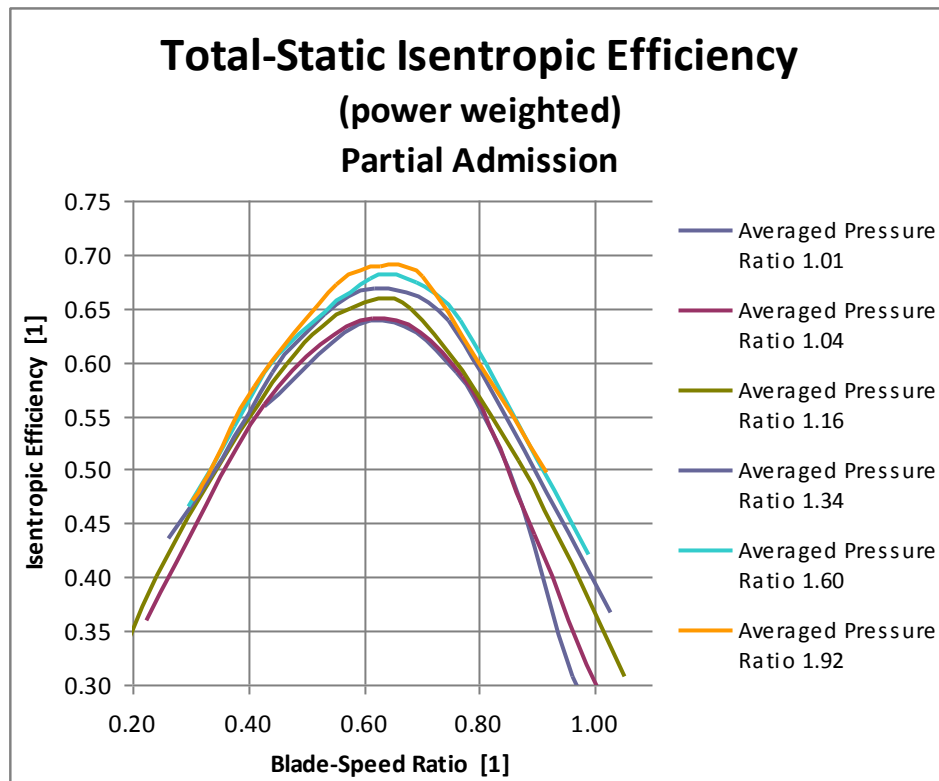


Fig. 23 Predicted BSR dependence of internal total-to-static isentropic efficiency of CZ K36 turbine – the largest trim for fixed 0.01 kg.s^{-1} (approx. averaged reduced mass flow-rate of $0.26 \text{ kg.s}^{-1}.\text{K}^{0.5}.\text{bar}^{-1}$) admission in the second partition of a twin scroll

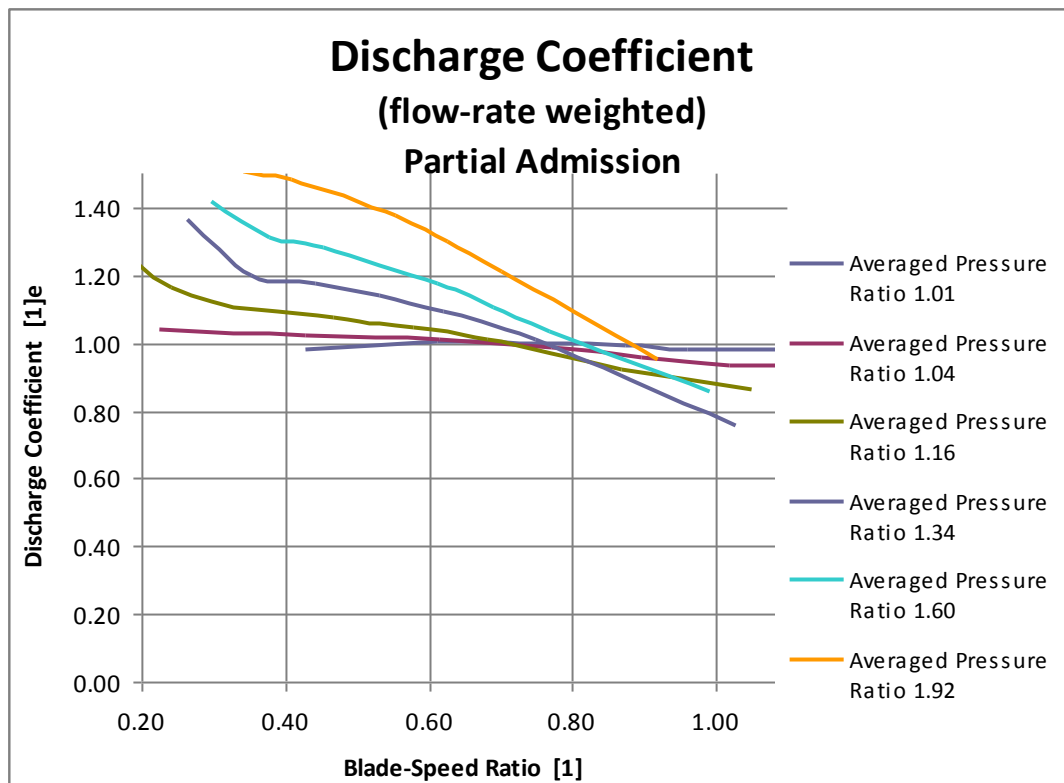


Fig. 24 Predicted BSR dependence of discharge coefficient for CZ K36 turbine – the largest trim (model calibrated by experiments) for fixed 0.01 kg.s^{-1} (approx. averaged reduced mass flow-rate of $0.26 \text{ kg.s}^{-1}.\text{K}^{0.5}.\text{bar}^{-1}$) admission in the second partition of a twin scroll. Reference cross-section area of 18 cm^2

Definitions, Acronyms and Abbreviations

SYMBOLS

| | |
|-------------------------------|---|
| A: | flow area [m^2] |
| a: | velocity of sound [m.s^{-1}] |
| b: | vane axial width [m] |
| C: | correction to compressibility [1] |
| c: | absolute velocity [m.s^{-1}] |
| c_p: | isobaric specific heat capacity [$\text{J.kg}^{-1}.\text{K}^{-1}$] |
| c_s: | velocity after isentropic expansion of a total enthalpy head, “isentropic velocity” [m.s^{-1}] |
| D: | diameter [m] |
| h: | specific enthalpy [J.kg^{-1}] |
| K: | tuning coefficient [1] |
| M: | torque [N.m] |
| m: | mass, mass flow rate (with dot) [kg, kg.s^{-1}] |
| n: | speed [min^{-1}] |
| P: | power [W] |
| p: | pressure [Pa] |
| Re: | Reynolds number [1] |
| r: | specific gas constant [$\text{J.kg}^{-1}.\text{K}^{-1}$] |
| r: | radius [m] |
| s: | specific entropy [$\text{J.kg}^{-1}.\text{K}^{-1}$] |
| T: | temperature [K] |
| u: | circumferential velocity [m.s^{-1}] |
| w: | relative velocity [m.s^{-1}] |
| x: | blade tip velocity ratio u_2/c_s [1] |
| z: | number of blades [1] |
| α: | angle of absolute velocity (measured from radial or axial direction) [deg] |
| β: | angle of relative velocity (measured from radial or axial direction) [deg] |
| ϵ: | pressure ratio <1 [1] |
| η: | isentropic efficiency [1] |
| κ: | isentropic exponent [1] |
| λ: | power input coefficient [1] |
| μ: | discharge coefficient |
| ν: | kinematic viscosity [$\text{m}^2.\text{s}^{-1}$] |
| π: | pressure ratio >1 [1] |
| ρ: | density [kg.m^{-3}] |
| τ: | shear stress [Pa] |
| ω: | angular velocity [rad.s^{-1}] |
| ψ: | flow function [1] |
| ζ: | kinetic energy loss coefficient [1] |

INDECES

| | |
|----------------|---|
| a: | axial |
| app: | approximation |
| comp: | compressible |
| F: | friction |
| I: | impeller |
| inc: | incidence, angle of attack |
| incomp: | incompressible |
| K: | compressor |
| leak: | leakage |
| N: | nozzle ring, vaneless turbine scroll&nozzle |

nom: nominal, at maximum efficiency
r: radial
red: reduced
rel: relative flow
s: isentropic
sep: flow separation
vent: windage
T: turbine
t: tangential
vl: vaneless
0: total state
1: inlet
2: outlet or nozzle ring outlet
3: impeller outlet
‘: blade root
“: blade tip

ACRONYMS

CR: centripetal radial
CRT: centripetal radial turbine
ICE: internal combustion engine
VG: variable geometry
VGT: variable geometry turbine
WG: waste-gate

Appendix 1

The Flow in Basic Passive Elements and Definition of Tuning Coefficients

Basic elements with flow acceleration or deceleration are described here. The total enthalpy h_o (or, in the case of perfect gas, the temperature T_o) is generally determined with relative flow velocity w . It is conserved in an adiabatic case if no work transfer occurs. This is the case of a rotating channel that is described in details in the body of the paper. The values of total parameters are designated by the index **0**; **1** stands for an inlet, **2** for an outlet of the element. Flow parameters can be simply calculated only if the total state upstream of an element and static downstream pressure are known.

If flow rate \dot{m} and inlet total temperature are known the method for determination of inlet or outlet pressures has to be used. It is useful especially for composed 1-D pipe systems. The method outlined here is versatile, giving possibilities to iterate directly unknown flow rates in serial-parallel channel systems.

The frequent general task is to find outlet static temperature and density if the flow rate, total inlet state and static outlet pressure are known. According to the standard definition an outlet total pressure p_{o2} is determined by

$$p_o = p \left(\frac{T_o}{T} \right)^{\frac{\kappa}{\kappa-1}}, \text{ i.e. } p_{o2} = p_2 \left(1 - \frac{w_2^2}{2c_p T_{o2}} \right)^{\frac{\kappa}{1-\kappa}} \quad (57)$$

The outlet velocity w_2 is calculated using continuity equation

$$w_2 = \frac{\dot{m}}{\rho_2 A_2} = \frac{\dot{m} r}{p_2} T_2 = \left(\frac{w_2}{T_2} \right) T_2 \quad (58)$$

and a conservation of energy yields with the velocity of sound $a = \sqrt{\kappa r T}$

$$h_o = h + \frac{w^2}{2} = \text{const.};$$
$$c_p T_{o1} = c_p T_1 + \frac{w_1^2}{2} = c_p T_2 + \frac{w_2^2}{2} \text{ or } \frac{a_{o1}^2}{\kappa-1} = \frac{a_2^2}{\kappa-1} + \frac{w_2^2}{2} \quad (59)$$

A quadratic equation for static outlet temperature yields :

$$\frac{1}{2} \left(\frac{w_2}{T_2} \right)^2 T_2^2 + c_p T_2 - c_p T_{o1} = 0 \quad (60)$$

T_2 , w_2 and p_{o2} can then be found this way.

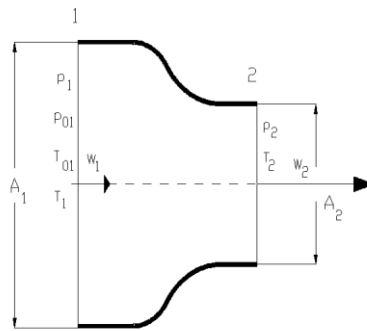
2-D Cases Transformed to 1-D

The tangential velocity component must be taken into consideration in turbomachinery. The second velocity component is directed to deliver gas into the machine (i.e., pure radial or axial direction in most cases according to the type of turbine). If no third-direction movement occurs the relations for total states are used with the resulting kinetic energy calculated from a total velocity

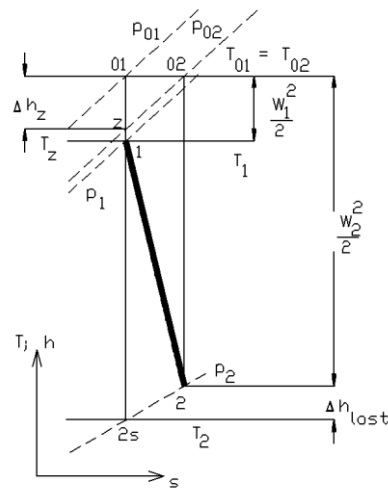
$$w^2 = w_t^2 + w_{a \text{ or } r}^2 \quad (61)$$

If the change of radius takes place angular momentum conservation has to be added to the set of the equations.

The Accelerated Flow in Nozzles



The variable and index notation has been chosen according to the Fig. 25. The entropy diagram in the Fig. 26 demonstrates the processes of compressible flow acceleration in both ideal and real cases and the definition of a loss coefficient.



Assuming the isobars are approximately parallel lines, the lost enthalpy head Δh_{lost} can be characterized by the head Δh_z :

$$\Delta h_{lost} = \frac{\zeta}{2} w_2^2 ;$$

$$\Delta h_z = c_p T_{01} \left[1 - \left(\frac{p_{02}}{p_{01}} \right)^{\frac{\kappa-1}{\kappa}} \right] \quad (62)$$

$$p_{01} = p_{02} \left\{ 1 - \zeta \left[1 - \left(\frac{p_2}{p_{02}} \right)^{\frac{\kappa-1}{\kappa}} \right] \right\}^{\frac{1-\kappa}{\kappa}} \quad (63)$$

Should the flow rate and outlet pressure be known, the equation (63) yields a total inlet pressure p_{01} . Using an initial estimation $p_1 = p_{01}$, the inlet static temperature T_1 and the velocity w_1 can be calculated in a way similar to (60). The last step is to find a more accurate static inlet pressure p_1 . The whole procedure is to be repeated until the required precision is achieved. This procedure is valid without corrections for subsonic region only.

To analyze the limits of subsonic region, let the upstream total states p_{01} and T_{01} together with the static outlet pressure p_2 are given. The outlet velocity is linked to the pressure ratio from (59) and (62) by

$$w_2 = \sqrt{2c_p(T_{01} - T_2)} = \sqrt{2c_p T_{01} \eta \left[1 - \left(\frac{p_2}{p_{01}} \right)^{\frac{\kappa-1}{\kappa}} \right]}, \quad \eta = \frac{1}{1 + \zeta_N}. \quad (64)$$

This equation defines an irreversible adiabatic change of state. It links temperatures and pressures well:

$$\left(\frac{T_2}{T_{01}} \right) = 1 - \eta \left[1 - \left(\frac{p_2}{p_{01}} \right)^{\frac{\kappa-1}{\kappa}} \right] \quad (65)$$

The sonic velocity limit for a convergent nozzle is given by the velocity of sound $w_2 = a_2$. The (59) yields the critical temperature ratio $\frac{2}{\kappa + 1}$. The corresponding limit of a pressure ratio is

$$\varepsilon^* = \left[1 - \frac{\kappa-1}{\eta(\kappa+1)} \right]^{\frac{\kappa}{\kappa-1}} < \left(\frac{p_2}{p_{01}} \right)_{subsonic} \quad (66)$$

It yields a well-known condition for an isentropic flow through an ideal nozzle with the unity efficiency. The mass flow rate is then for subsonic or sonic regimes

$$\dot{m} = \rho_2 A_2 w_{2\max}; \quad w_{2\max} = \begin{cases} w_2 \\ a_2 \end{cases} \quad (67)$$

$$\rho_2 = \begin{cases} \rho_{01} \frac{\varepsilon^*}{1 - \eta \left[1 - \varepsilon^{*\frac{\kappa-1}{\kappa}} \right]} \\ \rho_{01} \frac{p_2}{p_{01}} \frac{\varepsilon^*}{1 - \eta \left[1 - \left(\frac{p_2}{p_{01}} \right)^{\frac{\kappa-1}{\kappa}} \right]} \sqrt{2r \frac{\kappa}{\kappa-1} T_{01} \eta \left[1 - \left(\frac{p_2}{p_{01}} \right)^{\frac{\kappa-1}{\kappa}} \right]} \quad \text{if } \varepsilon^* = \left[1 - \frac{\kappa-1}{\eta(\kappa+1)} \right]^{\frac{\kappa}{\kappa-1}} < \frac{p_2}{p_{01}} \\ A_2 \frac{p_{01}}{rT_{01}} \frac{\varepsilon^*}{1 - \eta \left[1 - \varepsilon^{*\frac{\kappa-1}{\kappa}} \right]} \sqrt{2r \frac{\kappa}{\kappa-1} T_{01} \eta \left[1 - \varepsilon^{*\frac{\kappa-1}{\kappa}} \right]} \quad \text{otherwise} \end{cases} \quad (68)$$

Thus the sonic limit can be evaluated even in the case when significant losses are present, which is often the case of a turbine impeller.

The following iterative procedure is very useful if the unknown variables are other than the flow rate and static temperature and pressure upstream a turbine. A good estimation of a flow rate gives incompressible solution ($C_{comp}=1$) according to (69). It can be used also in algebraic equations, which are often solvable in the analytical form then. The precise values are

iterated using \dot{m} from realistic condition (68), which yields the actual value of C_{comp} . The whole procedure consists in a repetition of the following procedure starting with $C_{comp}=1$:

$$\dot{m}_{incomp} = \frac{A_2}{\sqrt{1 - \left(\frac{A_2}{A_1}\right)^2 + \zeta}} \frac{p_1}{\sqrt{rT_1}} \sqrt{2 \left(1 - \frac{p_2}{p_1}\right)} = \frac{A_2}{\sqrt{1 + \zeta}} \frac{p_{01}}{\sqrt{rT_1}} \sqrt{2 \left(1 - \frac{p_2}{p_{01}}\right)} \quad (69)$$

$$\dot{m} = C_{comp} \dot{m}_{incomp}$$

$$w_1 = \frac{\dot{m}}{A_1 \frac{p_1}{rT_1}} \quad (70)$$

$$T_{01} = T_1 + \frac{w_1^2}{2c_p}; \quad (71)$$

$$p_{01} = p_1 \left(\frac{T_{01}}{T_1} \right)^{\frac{\kappa}{\kappa-1}}; \quad \varepsilon = \frac{p_2}{p_{01}} \quad (72)$$

$$\psi = \begin{cases} \sqrt{\frac{2\kappa}{\kappa-1} \left(\varepsilon^{\frac{2}{\kappa}} - \varepsilon^{\frac{\kappa+1}{\kappa}} \right)} & \text{at } \varepsilon \geq \varepsilon^* \\ \sqrt{\frac{2\kappa}{\kappa-1} \left(\varepsilon^{*\frac{2}{\kappa}} - \varepsilon^{*\frac{\kappa+1}{\kappa}} \right)} & \text{at } \varepsilon < \varepsilon^* \end{cases} \quad (73)$$

$$C_{comp} = \frac{A_2}{\sqrt{1 + \zeta}} \frac{p_{01}}{\sqrt{rT_{01}}} \psi \frac{1}{\dot{m}_{incomp}} \quad (74)$$

This procedure has been applied just to the 2-D flow in the turbine. The problem solved by it is finding an unknown pressure between turbine cascades, the nozzle ring and the impeller. The condition of the same flow rates must be fulfilled if the pressure is correct.

Assuming the direction of flow (the exit flow angles), the kinetic energies and total states can be found from the continuity equation and the angles according to the Fig. 2.

The nozzle flow rate is described directly by (68). Assuming that the total state (p_{01} , T_{01}) upstream a turbine nozzle is known the outlet velocity has to be determined using (75) or (82) respectively. The definition of loss coefficient stated in (62) is used for blade cascades as well. Equivalent efficiency η is used again for the simplification of algebra. The other relations are obvious using the (71) and the state equation.

The flow rate estimation through a nozzle ring could be computed if static pressure p_{2N} is iteratively evaluated. The radial velocity and radial flow area (indexes r) have been used in (75) for the continuity equation at a nozzle ring exit.

$$c_2 = \sqrt{2c_p T_{01} \eta_N \left[1 - \left(\frac{p_{2N}}{p_{01}} \right)^{\frac{\kappa-1}{\kappa}} \right]}, \quad (75)$$

$$\eta_N = \frac{1}{1 + \zeta_N}$$

$$\rho_{2N} = \frac{p_{2R}}{r \left(T_{01} - \frac{c_2^2}{2c_p} \right)}; \quad (76)$$

$$\dot{m}_N = \rho_{2N} A_{r2N} c_2 \cos \alpha_2 = \dot{m}_{appN} C_N$$

The sonic limit treatment proceeds according to the (68).

The tuning coefficients are the outlet flow-rate-averaged angle and the efficiency of expansion. The effective flow area may be reduced by another flow-separation coefficient if necessary. It is not the standard case of turbine nozzles.

The C_N , a “compressibility” factor is used in an iterative solution of p_{2N} in the turbine model using an approximation in the sense of (69)- see (4) as well. The whole procedure yields the equation (4) if the model of a rotating channel is used. It will be described below.

A Vaneless Nozzle for a Radial Turbine

A vaneless nozzle is typical for small radial turbines. It accelerates a flow, changing the radius of a vortex inside the gap between side walls (usually parallel planes) – see FIG. 1 and FIG. 12, e.g., between 2'-2'' or 12 and 2N.

The tangential component of a flow velocity is created in a nozzle at the inlet to a turbine scroll. The nozzle axis is declined to a radial direction by an angle α_1 (usually 90 deg.) at the radius r_1 . The nozzle radial gap outlet is located at the radius r_{2N} of width b_2 .

The inlet tangential velocity component is

$$c_{t1} = c_1 \sin \alpha_1 = \frac{\dot{m}}{A_1 \rho_1} \sin \alpha_1 \quad (77)$$

The outlet velocity at a smaller radius increases according to an angular momentum conservation. The result should be corrected to a wall friction “braking” torque M_{loss} . It depends on the loss friction coefficient ζ_F :

$$c_{t2} r_2 = c_{t1} r_1 - \frac{M_{loss}}{\dot{m}} \quad (78)$$

$$M_{loss} = \int_1^2 r \tau_F dS = \int_1^2 r A dp_{loss} = \frac{1}{2} \frac{\dot{m}^2}{A_1 \rho_1} \int_1^2 \frac{r}{r_2} \zeta_F \frac{\rho_1 A_1}{\rho A} dx = K_F \frac{\dot{m}^2}{A_1 \rho_1} \frac{r_2}{r_1}$$

The wall friction torque is usually calculated transforming shear stress at walls to the “loss” of pressure due to friction. In most cases of vaneless turbine nozzles the structure of an inlet flow is not known in sufficient details. Then, combining (77) and (78) **the tuning coefficients may be integrated to the resulting K_{wI}**

$$\begin{aligned}
c_{t2}r_2 &= c_{t1}r_1 - K_{vf}c_{t2}r_2 \\
(1 + K_{vf})c_{t2}r_2 &= c_{t1}r_1
\end{aligned}
\tag{79}$$

The other tuning coefficient is an overall nozzle efficiency. The resulting outflow angle is calculated from tangential and total velocities in this case. Therefore it is not a new tuning coefficient.

$$\begin{aligned}
c_2^2 &= c_{r2}^2 + c_{t2}^2 = 2\eta_N \Delta h_{sN} = \\
&= 2\eta_N c_p T_{01} \left[1 - \left(\frac{p_2}{p_{01}} \right)^{\frac{\kappa-1}{\kappa}} \right]
\end{aligned}
\tag{80}$$

$$\alpha_2 = \arctg \frac{c_{t2}}{\frac{\dot{m}_T}{2\pi r_2 b_2 \rho_2}}
\tag{81}$$

This procedure substitutes blade nozzle simulation if a vaneless nozzle design is used (see (75), (76)).

The Flow in a Rotating Channel

The relative-motion total states have to be used together with the modified energy conservation according to (1).

The equations yielding a mass flow rate through a radial-axial impeller are deduced according to the (82). The easily calculated axial area (index **a**) of an exducer **3I** and an flow-rate-averaged outlet angle have been used. All flow areas should be, nevertheless, corrected to the blade thickness that should not be diminished especially in the case of small turbines. Another correction is called for by the frequent flow separation at a shroud in the region of maximum shroud curvature. All these factors are involved in a free-area reduction factor **K_{I sep}**.

$$\begin{aligned}
c_p T_3 + \frac{w_3^2}{2} - \frac{u_3^2}{2} &= c_p T_{rel02} - \frac{u_2^2}{2} \\
w_3 &= \sqrt{2c_p T_{rel02} \eta_I \left[1 - \left(\frac{p_3}{p_{rel02I}} \right)^{\frac{\kappa-1}{\kappa}} \right] + u_3^2 - u_2^2} \\
\rho_3 &= \frac{p_3}{r T_{rel02I}} \frac{p_{rel02I}}{1 - \eta_I \left[1 - \left(\frac{p_3}{p_{rel02I}} \right)^{\frac{\kappa-1}{\kappa}} \right]}
\end{aligned}
\tag{82}$$

$$\dot{m}_I = (1 - K_{I sep}) A_{a3I} \cos \beta_3 \rho_3 w_3 + \Delta \dot{m}_{leak} = \dot{m}_{appI} C_I
\tag{83}$$

The last relation contains beside an impeller channel flow additionally a leakage flow rate. All these unknowns may be incorporated in the definition of an iteration factor – a generalized “compressibility” coefficient **C_I** in the sense of (69). It simplifies the first approximation search as described in (4).

The sonic limit must be corrected to the influence of a centrifugal force because of the energy conservation law in a relative flow – (1). Thus

$$\varepsilon_I^* = \left[1 - \frac{1 - \frac{2}{\kappa + 1} \left(1 - \frac{\kappa - 1}{2a_{0rel}^2} (u_2^2 - u_3^2) \right)}{\eta_I} \right]^{\frac{\kappa}{\kappa - 1}} \quad (84)$$

The averaged flow exit angle, the expansion efficiency and the reduction of an exit free area due to a flow separation are the tuning coefficients of this case.

Decelerated Flow in Diffusers

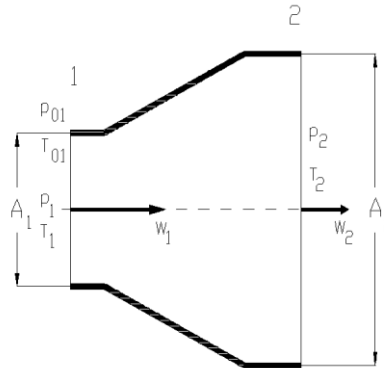


Fig. 27 The lay-out of a diffuser

A different approach must be applied for diffusers due to differences in a loss coefficient definition. A subsonic case is solved here. The scheme of a diffuser is shown in Fig. 27. An entropy diagram of the compression inside it with a loss coefficient definition is displayed at Fig. 28. The loss is defined according to the inlet kinetic energy using the lost enthalpy head again

$$\zeta = \frac{\Delta h_z}{\frac{1}{2} w_1^2} \quad (85)$$

which yields

$$p_{01} = p_{02} \left(1 - \frac{\zeta}{2} \frac{w_1^2}{c_p T_{01}} \right)^{\frac{\kappa}{1 - \kappa}} \quad (86)$$

An iterative procedure uses the initial state parameters estimated from the incompressible fluid flow, i.e. $p_{01} = p_{02}$; $T_1 = T_{02}$; $C_1 = C_2 = 1$. Both the latter coefficients correct pressures to the case of a compressible fluid during the iteration.

$$p_1 = C_2 p_{02} - \frac{C_1}{2} w_1^2 \rho_1, \quad i.e.,$$

$$p_1^2 - C_2 p_{02} p_1 + \frac{C_1}{2} \left(\frac{\dot{m}}{A_1} \right)^2 r T_1 = 0. \quad (87)$$

The approximation of p_1 is used for an estimate of T_1 based on an equation similar to (60) and for w_1 calculation. The correction for a real dynamic pressure can then be evaluated using the total pressure according to (57) and the solution of the 2nd relation (87)

$$C_1 = 2 \frac{p_{01}}{\frac{\rho_1}{r T_1} w_1^2} \left[1 - \left(1 - \frac{w_1^2}{2 c_p T_{01}} \right)^{\frac{\kappa}{\kappa-1}} \right] \quad (88)$$

The other correction for the ratio of total pressures is given by the definition of a loss coefficient

$$C_2 = \frac{p_{01}}{p_{02}} = \left[1 - \frac{\zeta}{2} \frac{w_1^2}{c_p T_{01}} \right]^{\frac{\kappa}{1-\kappa}} \quad (89)$$

The whole procedure, that is valid only in the case of a subsonic flow, is to be repeated. An isentropic subsonic condition is checked for the pressure ratio p_1/p_{01} . The solution for transonic domain is not required for the current simulation.

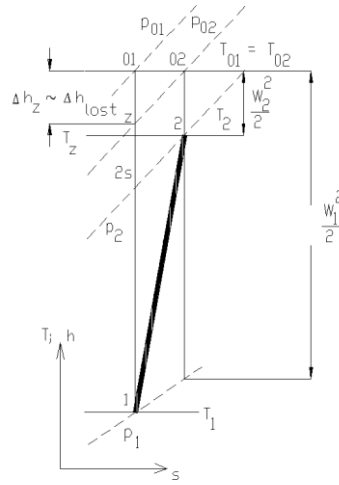


Fig. 28 Adiabatic irreversible compression in a diffuser

The tuning parameter is an efficiency coefficient. The effective flow area may be reduced by a flow-separation coefficient if necessary. It is not the standard case of turbine nozzles.

AN OUTLET axial-radial diffuser

A turbine outlet diffuser is frequently used downstream the impeller of a radial turbine. It is of advantage to create it in the axial-radial form. Then it converts even the kinetic energy delivered by a tangential velocity to the outlet static pressure.

2-D flow with neglected either radial or axial velocities according to the main direction of flow in the diffuser was developed amending the standard procedure (87) – (89) by an angular momentum conservation in an expanding flow with tangential velocity component. Kinetic energy, total enthalpy and losses are calculated for the total velocity composed of flow-rate-averaged axial component and radius-averaged tangential one using the assumed radial distribution of this velocity. Angular momentum conservation and averaging procedure for kinetic energy (from blade foot radius r' to tip one r'') yield

$$\int_{r_1'}^{r_1''} c_{t1} r dr = \int_{r_2'}^{r_2''} c_{t2} r dr - \frac{M_{loss}}{\dot{m}_T} \quad (90)$$

$$c_t = K.r^n \text{ for } n = 1; 0; -1;$$

$$c^2 = \frac{\int_{r_1'}^{r_1''} c_t^2 2\pi r dr + \left(\frac{\dot{m}}{\rho} \right)^2}{\pi(r_1''^2 - r_1'^2)}$$

The procedure has been tested for three different distributions (see n values). The most realistic ones according to measurement are those for both constant or to-radius-proportional tangential velocities. These results are not very different. The third case, potential vortex ($n=-1$) is very sensitive to the dimension of a vortex core where $n=1$. In the cases where a diffuser has no or a small-diameter central body, the potential vortex assumption gives unrealistic results.

Friction torque may be neglected assuming that both the velocity components are reduced uniformly in correspondence with overall losses.

As an amendment to this procedure, pressure difference and a mean static pressure between outer and inner diffuser contour should be integrated in presence of a centrifugal force field caused by a tangential velocity. It is of interest if the static pressure at the outer shroud is measured only (which is a frequent case) and these results are used for model calibration.

Tuning coefficients are so exponent of tangential velocity distribution, loss coefficient and outlet area reduction due to flow separation, which is present frequently.

Flow Junctions

The joining flows are typical for turbines with a twin-entry scroll used in pulse exhaust manifolds. The general junction equations can be used for this case with some specific changes.

The static pressures have to be calculated according to the momentum conservation in a junction. The other (total state) parameters are calculated in the neighboring elements of a pipe system according to the procedures described in the previous parts. The surfaces affected by the pressures in a junction are assumed to be of the same areas A_c (see Fig. 29). Moreover, both the inlet pressures are assumed to be the same in a subsonic domain. Then, the momentum equation is written for the single velocity component in the direction of a common pipe axis, which is taken into account by the cosines of axis angles measured from an outlet axis:

$$p_{IN,1} = p_{IN,2} = p_{OUT} + \frac{\dot{m}_{OUT} w_{OUT}}{A_c} - \frac{\dot{m}_{IN,1} w_{IN,1} \cos \alpha_1 + \dot{m}_{IN,2} w_{IN,2} \cos \alpha_2}{A_c} \quad (91)$$

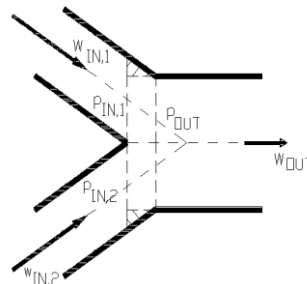


Fig. 29 Pipe (flow) junction

In the cases of flow junctions at turbines the angular momentum has to be used in the case of tangential velocity component with appropriate (often constant) radii similarly, as in the case of (90). An additional torque loss may be taken into consideration, acting on the flow. It is negligible in the cases, if no vanes are used and a friction in boundary layers is not dominant.

Incidence Loss of a Turbine Impeller

The last linking condition considers static pressures at a nozzle outlet **2N** and an impeller inlet **2I**. An empirical equation for a pressure loss due to the off-design incidence angle at impeller (radial) blades has to be added because there may be a difference between static pressures at nozzle exit and impeller inlet - see Fig. 1, Fig. 3.

The simplest approach for radial blades considers a dissipation of all kinetic energy associated with a tangential relative velocity component (Benson, $\zeta_{Ii} = \tan \beta_{2i}$, see e.g. [1]). Usually, $\beta_{2i} = \beta_2$ was used. The experimental results call for correction of this approach, as stated already in [3], preferring the negative angles of attack by a positive coefficient K_{imp} :

$$\zeta_{Ii} = 2 \frac{p_{0rel2N} - p_{0rel2I}}{\rho_2 w_{2I}^2} = (\tan \beta_2 + K_{imp})^2 \quad (92)$$

$$p_{0rel2I} = p_{0rel2N} - \frac{\zeta_{inc} w_{2I}^2 \rho_{2I}}{2}; \quad T_{2I} = T_{2N} + \frac{w_{2N}^2 - w_{2I}^2}{2c_p} \quad (93)$$

$$p_{2I} = p_{0rel2I} \left(\frac{2c_p T_{2N} + w_{2N}^2 - w_{2I}^2}{2c_p T_{2N} + w_{2N}^2} \right)^{\frac{\kappa}{\kappa-1}}; \quad \rho_{2I} = \frac{p_{2I}}{r T_{2I}}$$

This correction can be proven from the relative vortex motion inside an impeller channel (slip of the flow peculiar to radial machines). Using the classic Stodola estimation of the vortex circumferential speed from an inlet distance between vanes and from an angular velocity of a turbine impeller, the flow is declined opposite to the sense of rotation by an angle $\Delta\beta_2$

$$\tan \Delta\beta_2 = \frac{\Delta w_{t2}}{w_{r2}} = -\omega_I \frac{\pi \cdot D_{2I}}{Z} = -u_2 \frac{\pi}{Z} \quad (94)$$

Therefore, the optimum angle of incidence is not a radial one then. It should be increased by $-\Delta\beta_2$ to compensate for relative vortex influence. Thus for radial vanes with an empirical correction K_{inc} of Stodola's estimation

$$\zeta_{Ii} = \left(\frac{w_{t2} - K_{inc} \Delta w_{t2}}{w_{r2}} \right)^2 = (\tan(\beta_2 - \Delta\beta_2))^2 =$$

$$= \left(\frac{\tan \beta_2 - K_{inc} \tan \Delta\beta_2}{1 + \tan \beta_2 \tan \Delta\beta_2} \right)^2 \doteq (\tan \beta_2 - K_{inc} \tan \Delta\beta_2)^2 \quad (95)$$

This is roughly equivalent to (92) for usual $\Delta\beta_2 < 0$. Nevertheless, in this case the correction should be proportional to turbine speed. The calibration procedure will find, whether original Benson proposal or Stodola vortex based approach is more relevant. K_{inc} becomes a new tuning parameter. With $K_{inc} = \text{const.}$ it gives less off-design incidence loss increase than according to (92).

Appendix 2 – Examples of Turbine Models Built by Entities of 1-D Code

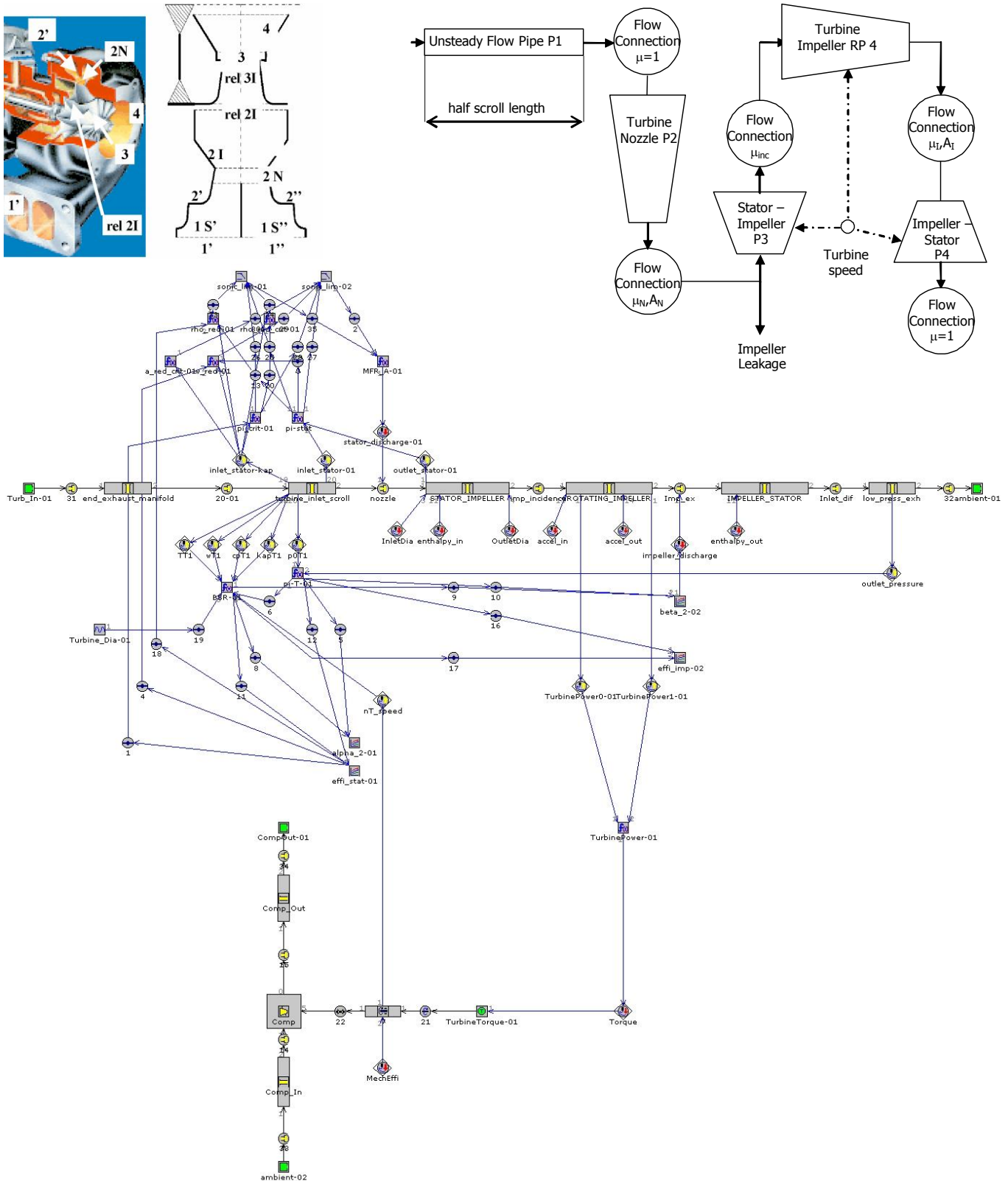
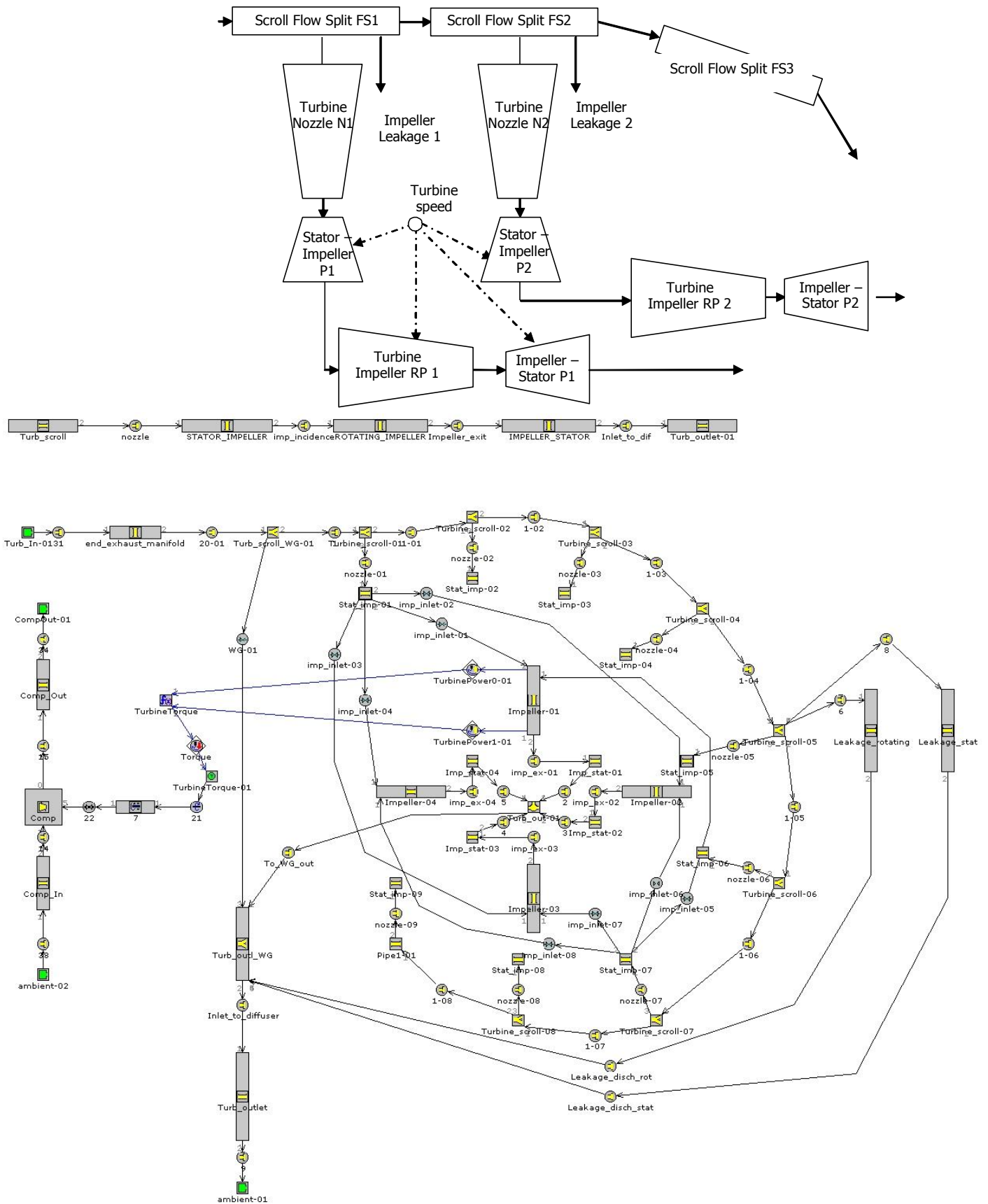


Figure 1 Initial model scheme of a radial turbine with averaged dimensions of components (e.g., scroll volute represented by the mean length of the flow path). 1-D schematic models attached above for comparison with GTP model lay-out.



3. Dixon, S.L.: FLUID MECHANICS, THERMODYNAMICS OF TURBOMACHINERY. Pergamon Press, Oxford 1975
4. Topercer, P., Hubáček, T., Kundera, R.: MEASUREMENTS AT TURBINE PTR150 (IMPELLER DIAMETER 150 MM) AND AUTOMOTIVE ONE K36 (DIAMETER 96MM) USING HIGH-SPEED DYNAMOMETER IN THE BROAD RANGE OF PRESSURE AND VELOCITY RATIOS. In Czech. Internal Research Reports PBS Velká Bíteš 1999 and 2000, 250 pp.
5. Prostějovský, D. - Macek, J.: METHODOLOGY OF TURBOCHARGER CHARACTERISTICS MEASUREMENT. In Czech. Research Report of CTU FS K221 Z 98-12, Praha 1998, 34 pp.
6. Vávra, J. - Macek, J.: EVALUATION OF K36 A C14 TURBINE CHARACTERISTICS (MANUFACTURER ČZ STRAKONICE). In Czech. Research Report of CTU FS K221 Z 99-10, Praha 1999, 65 pp.
7. Polášek, M. - Macek, J.: ON THE POSSIBILITIES OF TURBOCHARGING OF A SMALL AUTOMOTIVE DIESEL. IN: Conference KOKA 2000. Žilina: Technical University of Žilina. 2000. p. 177-182. - ISBN 80-7100-736-6
8. Zinner, K.: Supercharging of Internal Combustion Engines. Springer Heidelberg 1978
9. Winterbone, D.E. et al.: A Contribution to the Understanding of Turbocharger Turbine Performance in Pulsating Flow. Int. Conf. on Internal Engine Research, Paper C433/011, Instn.Mech.Engrs. London 1991
10. Lujan, J.M., Galindo, J., Serrano, J.R.: Efficiency Characterization of Centripetal Turbines under Pulsating Flow Conditions. SAE Paper 2001-01-0272
11. GT-POWER User's manual and Tutorial GT-Suite™ version 6.2, 2006, Private Publication.
12. Lawless, P.B.: Characterization and Modeling of Turbocharger Dynamic Performance. SAE Paper 97 1566
13. Gurney, D.: The Design of Turbocharged Engines Using 1-D Simulation. SAE Paper 2001-01-0576
14. Capobianco, M., Marelli, S.: Turbocharger Turbine Performance Under Steady and Unsteady Flow: Test Bed Analysis and Correlation Criteria. 8th Intl. Conf. on Turbochargers and Turbocharging, IMechE London, 2006
15. Capobianco, M., Marelli, S.: Unsteady Flow Behaviour of the Turbocharging Circuit in Downsized Automotive Engines. FISITA Congress 2006, Yokohama, paper F2006P119, 12 pp.
16. Capobianco, M., Marelli, S.: Transient Performance of Automotive Turbochargers: Test Facility and Preliminary Experimental Analysis. SAE Paper 2005-24-66
17. Capobianco, M., Gambarotta, A.: Variable Geometry and Waste-Gated Automotive Turbochargers: Measurements and Comparison of Turbine Performance. Journal of Engineering for gas Turbines and Power, Volume 114, 1992, pp. 553-560
18. Costall, A., Szymko, S., Martinez-Botas, R.F., Filsinger, D., Ninkovic, D.: Assessment of Unsteady Behaviour in Turbocharger Turbines. Proceedings of ASME TurboExpo 2006, pap. GT2006-90348, Barcelona 2006
19. Winkler, N., Angstrom, H.E., Olofsson, U.: Instantaneous On-Engine Twin-Entry Turbine Efficiency Calculations on a Diesel Engine. SAE Paper 2005-01-3887
20. Winkler, N., Angstrom, H.E., Olofsson, U.: Instantaneous On-Engine Turbine Efficiency for a SI Engine in the Closed Waste Gate Region for 2 Different Turbochargers. SAE Paper 2006-01-3389
21. Westin, F., Angstrom, H.E.: Calculation Accuracy of Pulsating Flow through the Turbine of SI-Engine Turbochargers – Part 1. SAE Paper 2005-01-0222
22. Hu, Xiao, Lawless, P.B.: Predictions of On-Engine Efficiency for the Radial Turbine of a Pulse Turbocharged Engine. SAE Paper 2001-01-1238
23. Osako, K., Higashimori, H., Mikogami, T.: Study on the Internal Flow of Radial Turbine Rotating Blades for Automotive Turbochargers. SAE Paper 2002-01-0856
24. C. Ciesla, R. Keribar and T. Morel, "Engine/Powertrain/Vehicle Modeling Tool Applicable to All Stages of the Design Process", SAE 2000 Congress, Paper 2000-01-0934.
25. T. Morel, R. Keribar and A. Leonard, "Virtual Engine/Powertrain/Vehicle Simulation Tool Solves Complex Interacting System Issues", SAE Paper 2003-01-0372
26. Vítek, O., Macek, J., Polášek, M.: New Approach to Turbocharger Optimization using 1-D Simulation Tools. SAE Paper 2006-01-0438, SAE Int. Warrendale 2006, 15 pp.
27. Navrátil, J., Macek, J., Polášek, M.: Simulation of a Small Turbocharged Gasoline Engine in Transient Operation. SAE Paper In Modelling of Spark Ignition Engines. Warrendale, PA 15096: SAE International, 2004. ISBN 0-7680-1366-6.
28. Macek, J. - Vávra, J. - Vítek, O.: 1-D Model of Radial Turbocharger Calibrated by Experiments. SAE Paper 2002-01-0377.. In: Modeling of SI Engines and Multi-Dimensional Engine Modeling. Warrendale, PA : Society of Automotive Engineers, 2002, vol. 1, p. 173-194. ISBN 0-7680-0970-7.
29. Pohořelský, L. - Macek, J. - Polášek, M. - Vítek, O.: Simulation of a COMPREX Pressure Exchanger in a 1-D Code. SAE Paper 2004-01-1000. In Modeling of Spark Ignition Engines. Warrendale, PA 15096: SAE International, 2004, vol. 1. ISBN 0-7680-1366-6.
30. Salkin, A.: Utilization of modeFrontier as a Calibration Tool for Mechanical Models. CVUT Prague/ECN Nantes 2006. Internship Report, unpublished.